



Exploring 3D-QSAR to Identify Potential Small Molecule for Treating Alzheimer Disease: A Case Study With β -Secretase Inhibitors

Uttam A More,¹ Maitri Patel,¹ Krishna Patel,¹ Harsiddhi Patel,¹ Kruti Y Patel,¹ Neha Jain,¹ Shabeena Khan,¹ Kinjal Vasandiya,¹ Malleshappa N Noolvi,¹ Mahesh B Palkar²

Abstract

Background/Aim: One of the most common neurological conditions that results in dementia is Alzheimer disease. The current treatment options for Alzheimer disease include acetylcholinesterase (AChE) and -methyl-D-aspartate (NMDA) inhibitors, but there is a significant need for further research. There are numerous molecular targets that can be used to treat Alzheimer disease. Aim of this study was to analyse β -secretase as a target because of its documented involvement in the pathophysiology of the illness. Additionally, prior research investigated the possible therapeutic effects of derivatives based on guanidine.

Methods: A total of 146 well-known β -secretase inhibitors were collected from various literature sources. To forecast these compounds' inhibitory potency, models were created using ligand-based drug design (LBDD) and quantitative structure-activity relationship (3D-QSAR) investigations. Six models were generated and based on the statistical parameters q^2 (cross-validated R^2) and standard error of estimate (SEE), the 6th model was selected for further investigation.

Results: A cross-validated R^2 (R^2_{cv}) value of 0.764 was obtained utilising the leave-one-out (LOO) method in the partial least squares (PLS) analysis for atom-based QSAR. With an F ratio of 337.2, a SEE of 0.2306 and an R^2 value of 0.9516, the non-cross-validated analysis produced these results. Field-based QSAR had an R^2_{cv} value of 0.7353, while the non-cross-validated analysis produced an F ratio of 283.1, an R^2 value of 0.9428 and a SEE of 0.2505. Predicting the inhibitory potency of novel compounds against β -secretase was done using the contour map analysis. Atom-based and field-based 3D-QSAR models projected the pIC_{50} value of the proposed compound P1 to be 8.41 and 8.32, respectively.

Conclusion: The findings of this study provide valuable insights into the design of new molecules targeting β -secretase in Alzheimer disease. The predictive models and the newly designed molecules, particularly molecule P1, could serve as potential leads for the development of new chemical entities as anti-Alzheimer agents. These results may significantly contribute to the ongoing efforts to develop more effective treatments for Alzheimer disease.

Key words: Alzheimer disease; Pharmaceutical preparations; Quantitative structure-activity relationship; Amyloid precursor protein secretases, antagonists and inhibitors; Guanidine.

1. Department of Pharmaceutical Chemistry, Shree Dhanvantary Pharmacy College, Kim, Surat, Gujarat, India.
2. Department of Pharmaceutical Chemistry, Shobhaben Pratapbhai Patel School of Pharmacy and Technology Management SVKM's Narsee Monjee Institute of Management Studies University (NMIMS), Vile Parle (W), Mumbai, Maharashtra, India.

Citation:

More UA, Patel M, Patel K, Patel H, Patel KY, Jain N, et al. Exploring 3D-QSAR to identify potential small molecule for treating Alzheimer disease: a case study with β -secretase inhibitors. Scr Med. 2025 Jul-Aug;56(4):625-58.

Corresponding author:

UTTAM A MORE
E: uttamsvd@gmail.com
T: +91 8401841577

Received: 4 January 2025

Revision received: 16 February 2025

Accepted: 16 February 2025

Introduction

Alzheimer disease (AD) is a neurodegenerative disease that primarily affects the elderly population worldwide. It is progressive and currently incurable. Short-term memory loss, speech impairment, decreased motor skills, poor coordination and diminished cognitive abilities are some of the symptoms of this most prevalent type of dementia.¹

Approximately 6.7 million Americans 65 and older currently suffer from Alzheimer dementia and unless there are major medical advancements that could prevent, slow, or cure the disease, this number is expected to rise to 13.8 million by 2060.² A persistent deterioration in short-term memory and cognitive abilities is one of the early signs of AD, which is usually accompanied by behavioural abnormalities like depression and aggression.³ The cholinergic, tau and amyloid hypotheses are among the theories put forth to explain the pathophysiology of AD. While these theories provide insights into the disease's progression, none fully explain its underlying cause.⁴ However, they have been instrumental in developing potential treatment strategies aimed at slowing AD progression.⁵ Among these hypotheses, the amyloid hypothesis is the most prominent. It suggests that the buildup of amyloid- β (A β) peptides in the brain is what causes AD. The main components of amyloid plaques, these peptides are usually 39–43 amino acids long and are thought to start a neurotoxic cascade that eventually leads to dementia and neuronal death. Two aspartic proteases, β -secretase (BACE1) and γ -secretase, sequentially cleave the membrane-bound amyloid precursor protein (APP) to produce A β peptides. The first cleavage of APP, which results in the membrane-bound carboxy-terminal fragment (C99) and the secreted amino-terminal fragment (sAPP β), is caused by BACE1. Toxic A β peptides are created when γ -secretase further cleaves the C99 fragment.⁴⁻⁶

Genetic alterations in APP have been associated with both early-onset AD and protection against the disease, underscoring the importance of the amyloid pathway and A β production in AD pathogenesis. In order to stop or decrease A β production and, consequently, treat AD, BACE1 inhibition has become a viable therapeutic approach.^{7,8} Comprehending the mechanism of interaction between β -secretase and its inhibitors is essential for creating small molecule inhibitors that can efficiently target this enzyme. Numerous experimentally determined three-dimensional structures of β -secretase, both by itself and in combination with different inhibitors (like Lol-Alq-based peptidomimetic inhibitors), offer important information for drug discovery efforts that aim to stop

β -secretase activity and thereby slow the progression of AD.⁹⁻¹²

Lead compound discovery and chemical analogue optimisation for a range of biological activities have greatly benefited from recent developments in quantitative structure-activity relationship (3D QSAR) methodologies. To identify the structural features critical for enhanced activity against B-secretase, 3D-QSAR studies were performed on a set of 146 guanidine-containing compounds. The well-known 3D QSAR techniques include comparative molecular field analysis (CoMFA)¹³ and comparative molecular similarity indices analysis (CoMSIA).¹⁴ CoMFA focuses on the steric and electrostatic fields, while CoMSIA expands the analysis to include hydrogen bond acceptor, hydrogen bond donor and hydrophobic fields. Field-based QSAR techniques, such as those used in CoMSIA, utilise these five descriptors, while atom-based QSAR methods cover additional descriptors, including hydrogen bond donor, hydrophobic, negative ionic, positive ionic and electron-withdrawing fields. In the present study, both field-based and atom-based QSAR techniques were employed to create a common 3D lattice around these molecules. This lattice enabled the calculation of steric and electrostatic interaction energies, as well as Gaussian-based similarity functions.¹⁵ To elucidate the correlation between the structure of guanidine derivatives and their biological activity, initially, 146 guanidine-based derivatives with known β -secretase inhibitory activity were collected to construct the 3D QSAR models. The application of Lennard-Jones and Gaussian-based approaches provided insights into the contributions of both favourable and unfavourable regions to the compounds' biological activity.^{16,17} Utilising this knowledge, a novel molecule and predicted its potential as a β -secretase inhibitor was designed.

Methods

Data collection

To investigate potential BACE-1 inhibitors, a dataset of 146 compounds containing a common guanidine fragment (1-129) and its bioisostere acetimidic acid and acetamide fragment (130-146) was curated from the ChEMBL database. These inhibitors exhibited potent activity with IC₅₀ values ranging from 8 to 5500 nM. The experimental IC₅₀ values were converted to their corresponding negative logarithmic values (pIC₅₀)

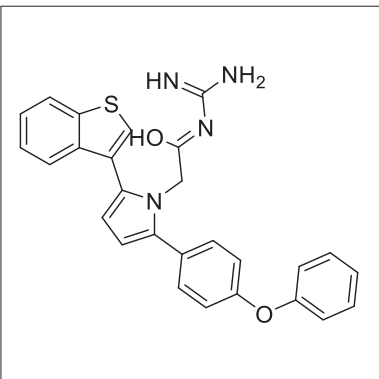
using the formula $\text{pIC}_{50} = 9 - \log_{10}(\text{IC}_{50})$ and all compounds with pIC_{50} values within this range were included in the study, as detailed in Table 1. The 2D structures of these compounds were initially checked using *ChemDraw* which were obtained from *ChEMBL* database. Subsequently, the geometry of each molecule was optimised using the LigPrep module in *Schrodinger Maestro* software.^{15, 18} The preparation parameters included the use of the OPLS 2005 force field, consideration of all possible ionisation states at physiolog-

ical pH, generation of potential tautomers, maintenance of original stereochemistry based on the number of chiral centres and generation of one low-energy ring conformation per ligand.¹⁹ These prepared molecules were then utilised for the development of 3D-QSAR models. The 3D-QSAR calculations, based on Gaussian distributions, were performed for all compounds using *Schrodinger Maestro*. The details of the training and test set molecules, along with their experimental IC_{50} values, are presented in Table 1.

Table 1: Chemical structure of selected guanidine-based derivatives and its BACE-1 inhibitory potency

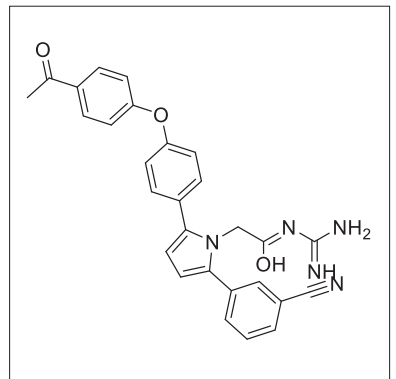
SN	Chemical structure	IC_{50}	SN	Chemical structure	IC_{50}
1		500	2		600
3		600	4		600
5		600	6		700

7



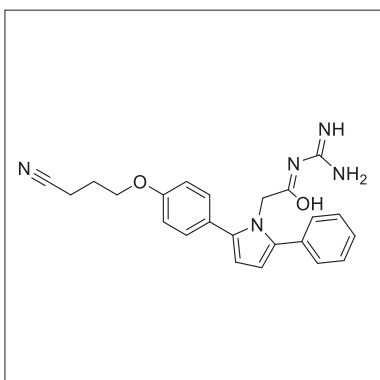
700

8



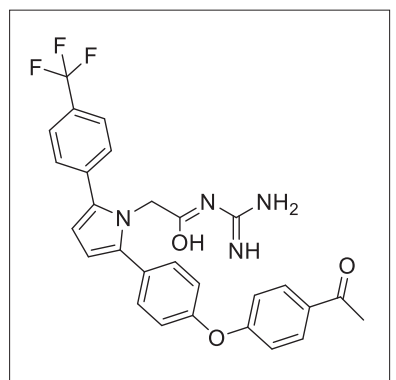
800

9



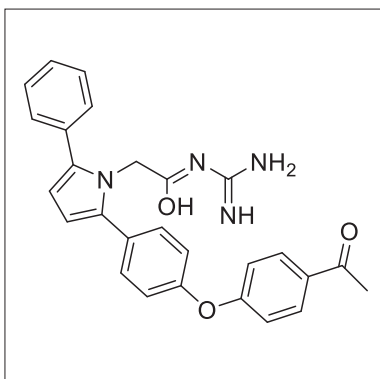
900

10



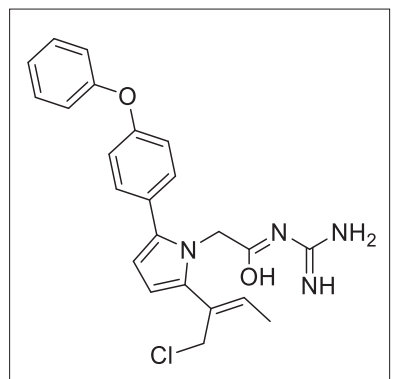
900

11



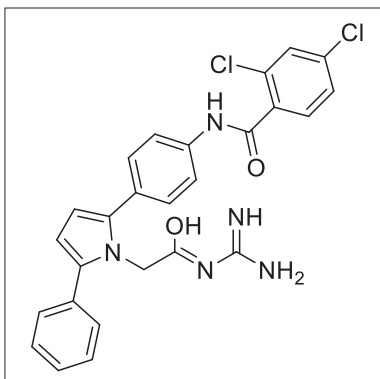
1000

12



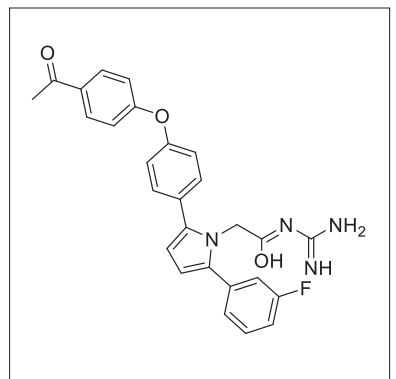
1100

13



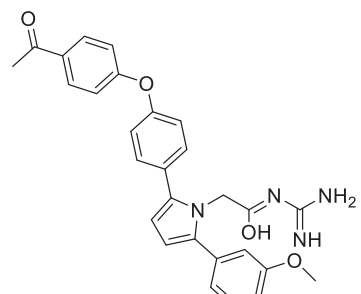
1200

14



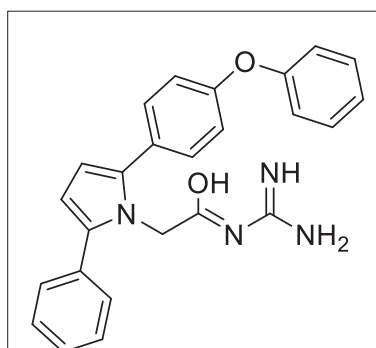
1200

15



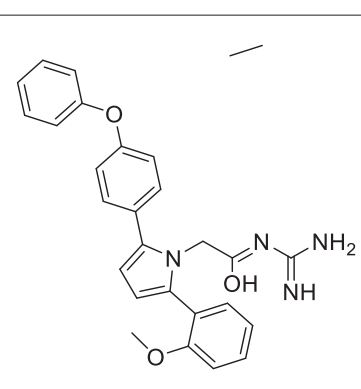
1300

16



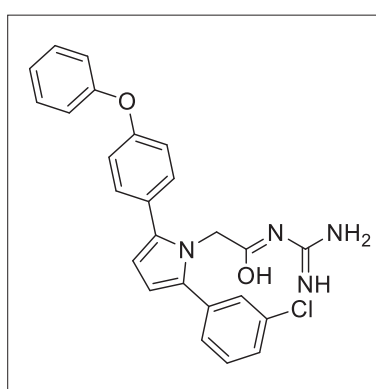
1300

17



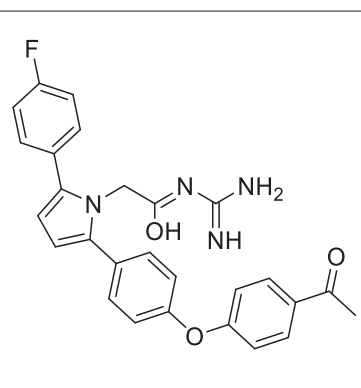
1300

18



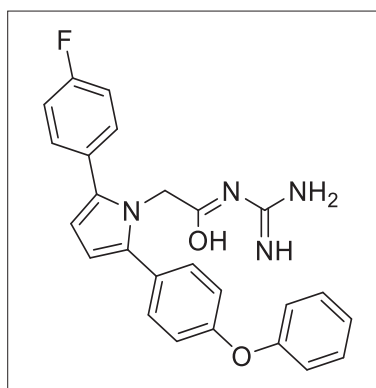
1300

19



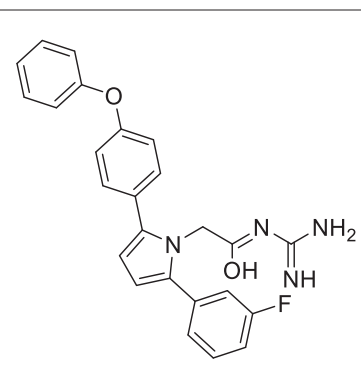
1300

20



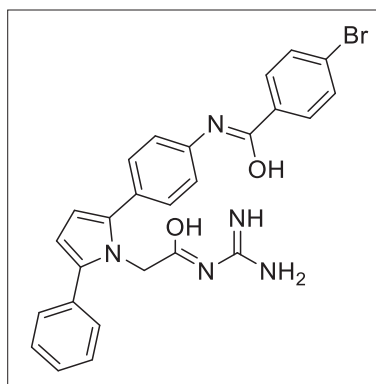
1400

21



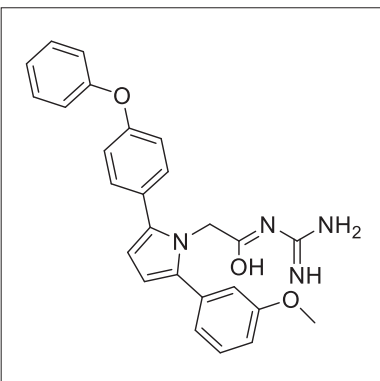
1400

22



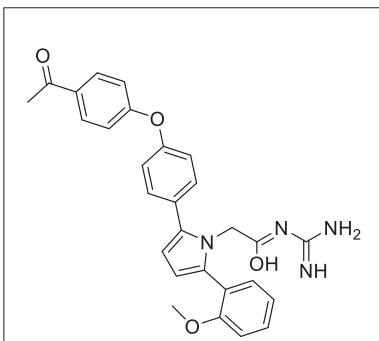
1400

23



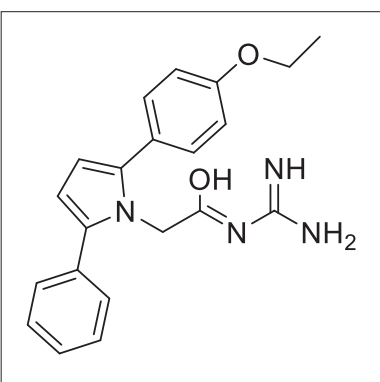
1500

24



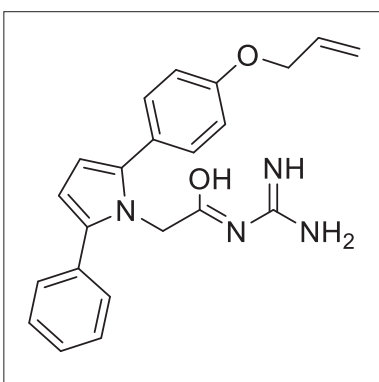
1600

25



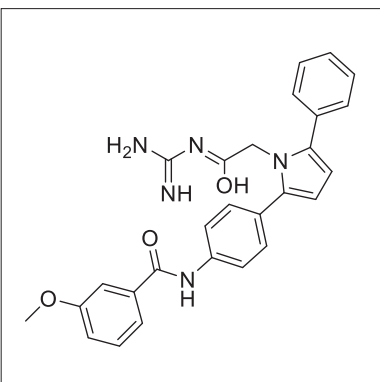
1600

26



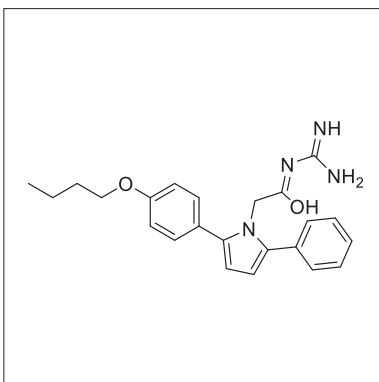
1700

27



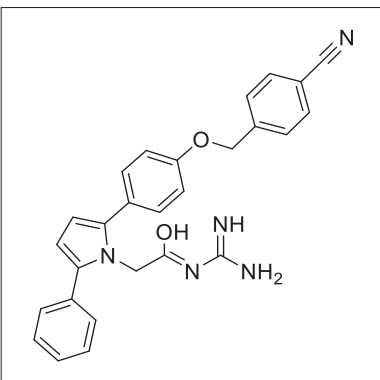
1800

28



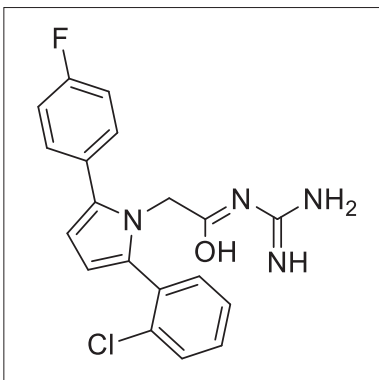
1800

29



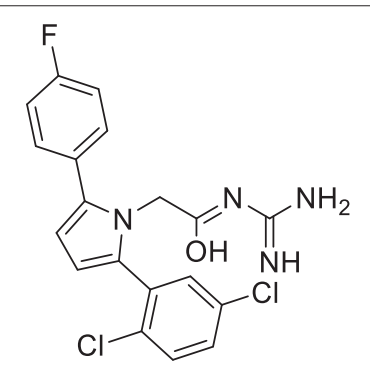
1900

30



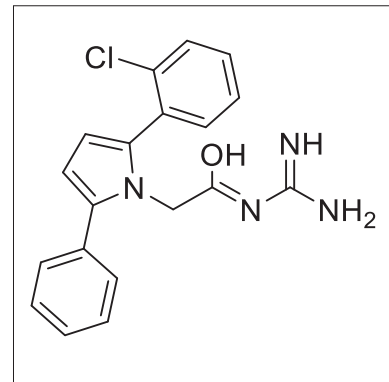
2000

31



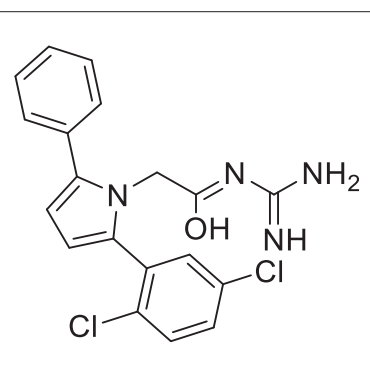
2000

32



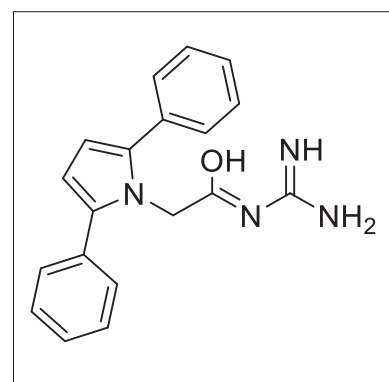
3000

33



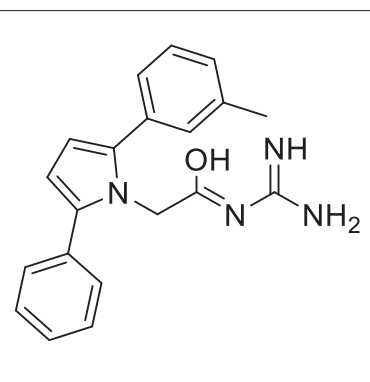
3500

34



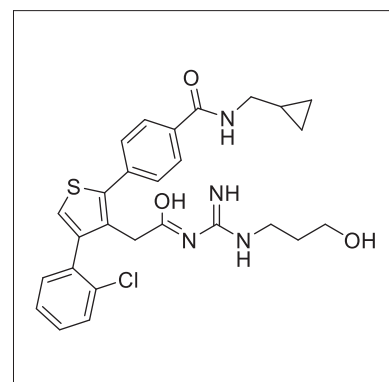
3700

35



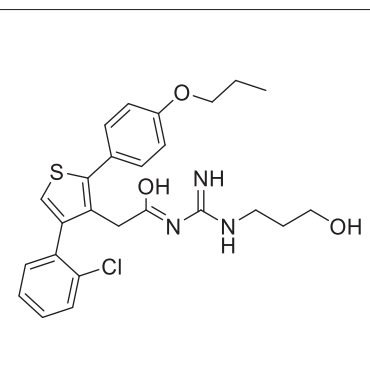
4600

36



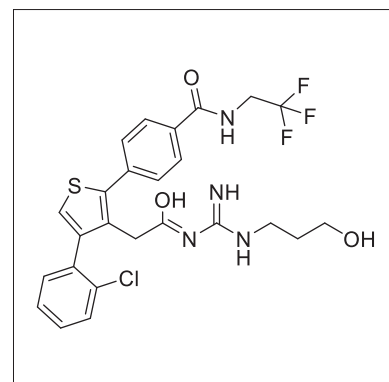
140

37

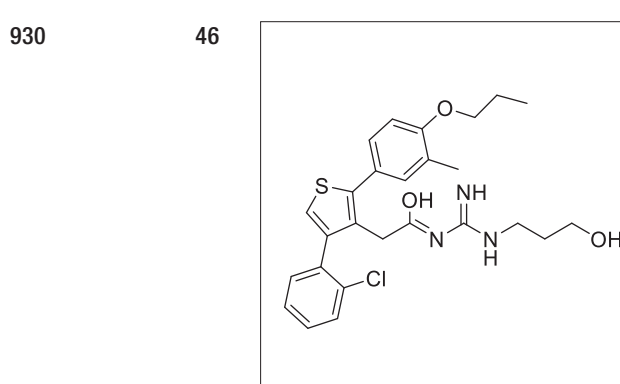
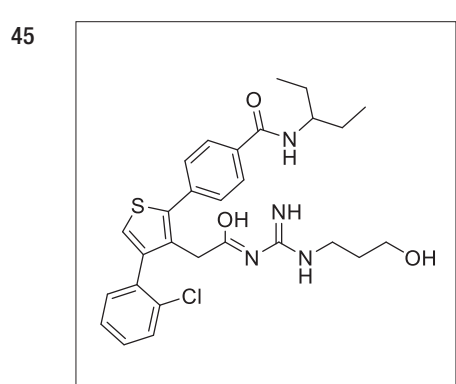
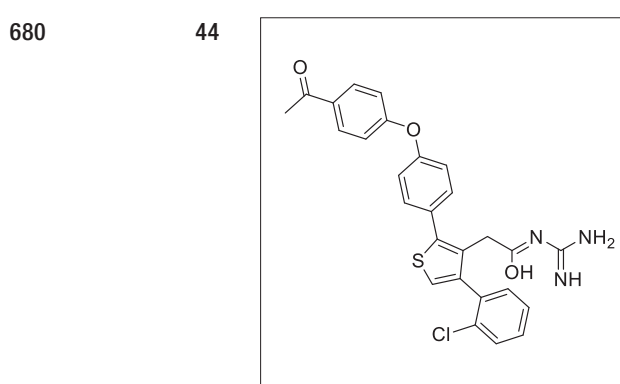
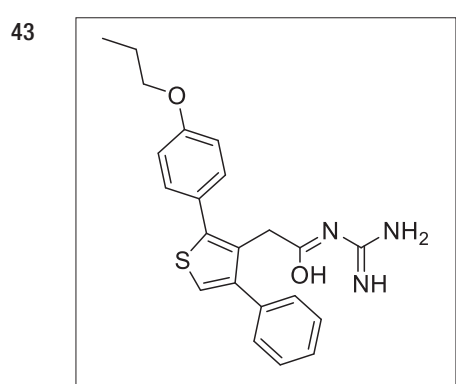
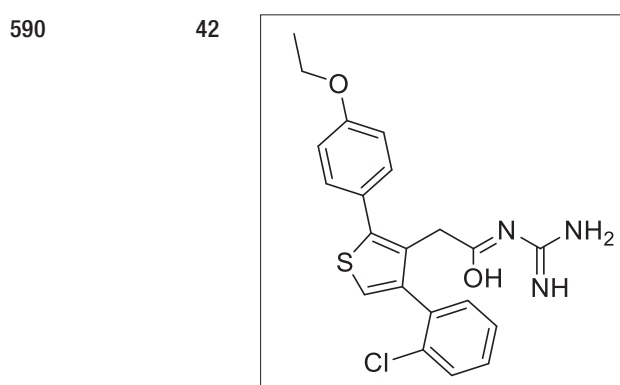
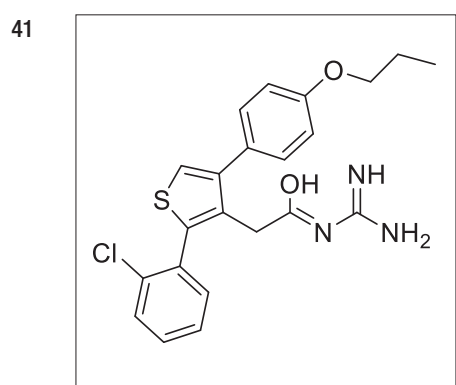
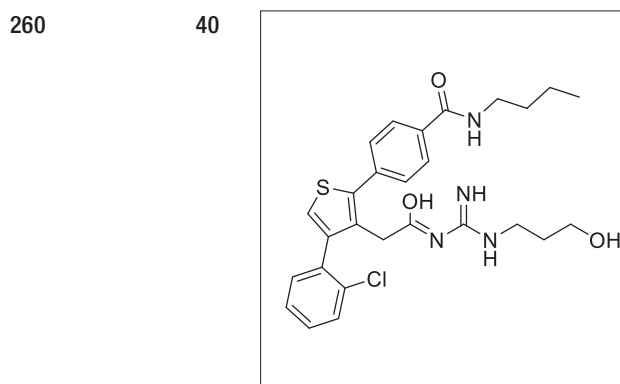
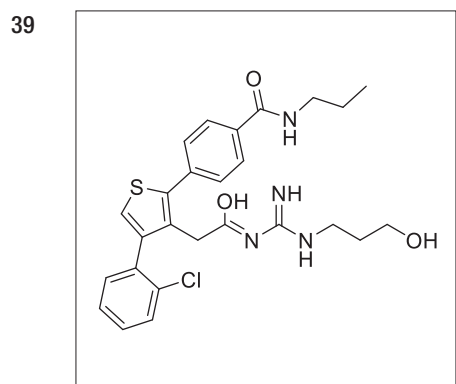


150

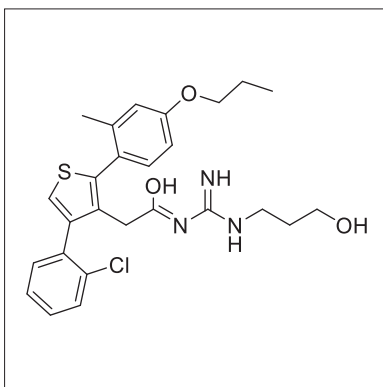
38



200

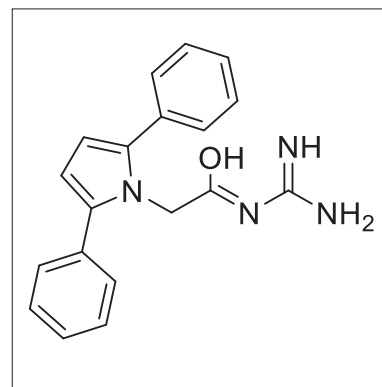


47



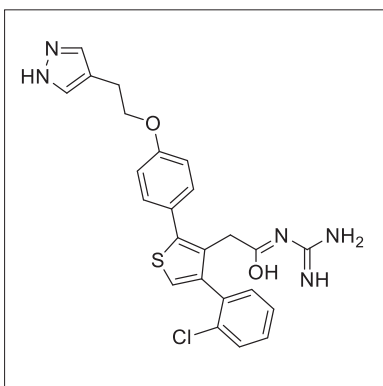
1550

48



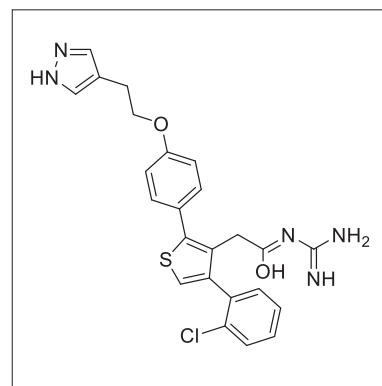
1890

49



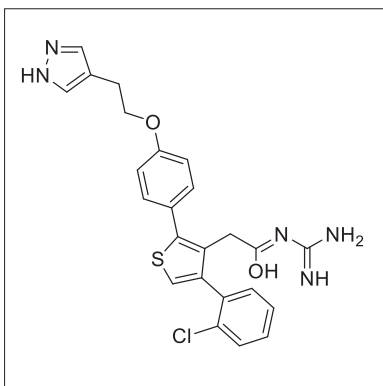
3700

50



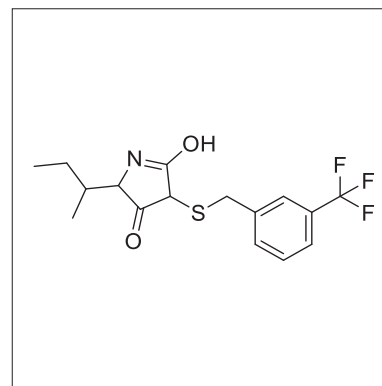
6900

51



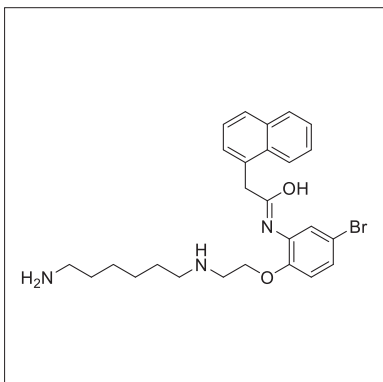
8300

52



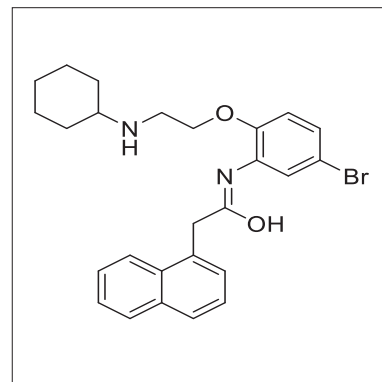
60000

53



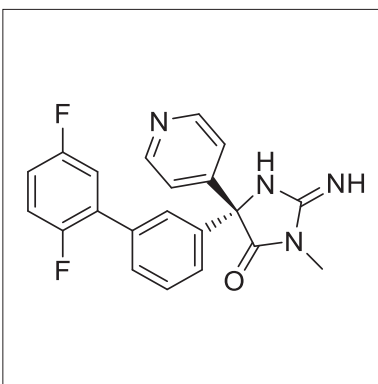
18

54



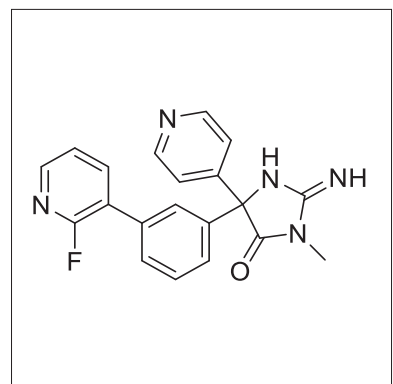
47

55



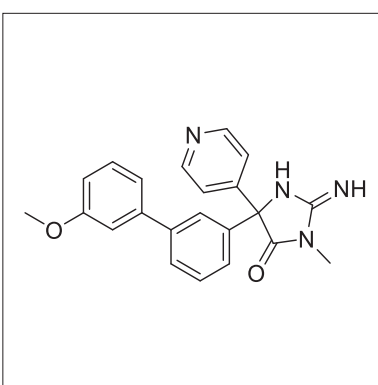
20

56



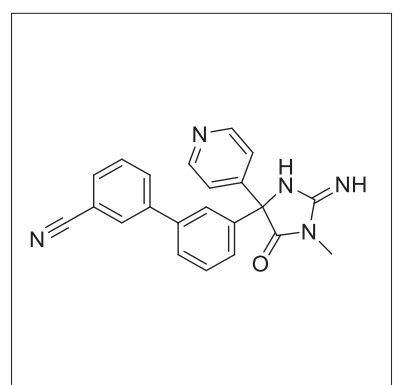
30

57



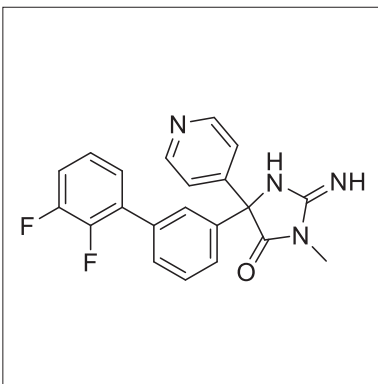
30

58



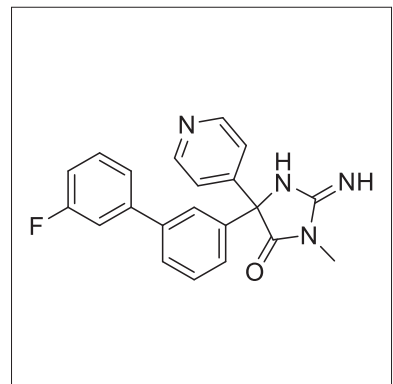
40

59



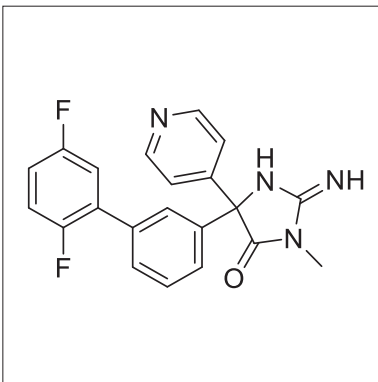
40

60



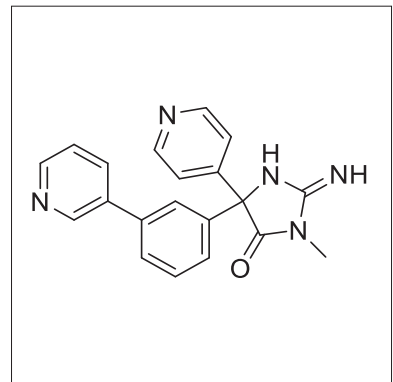
50

61

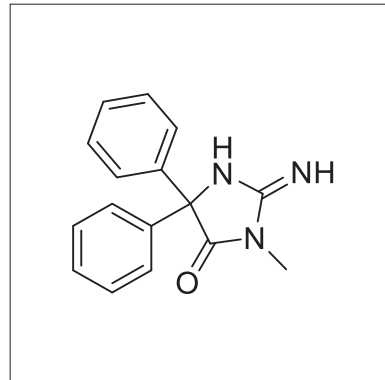
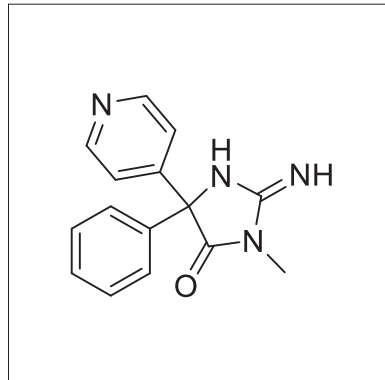
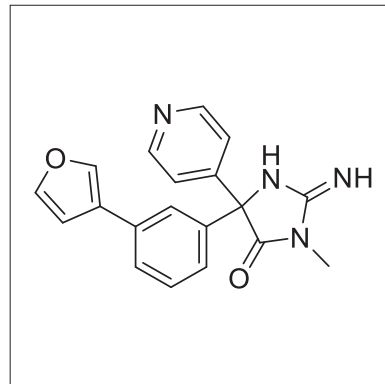
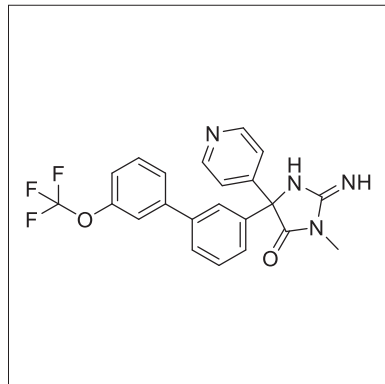
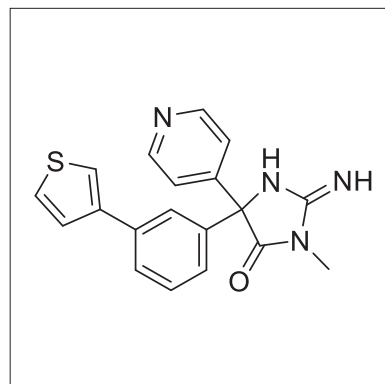
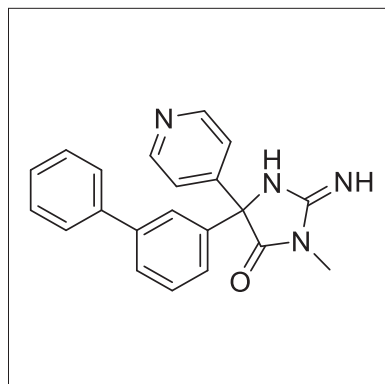
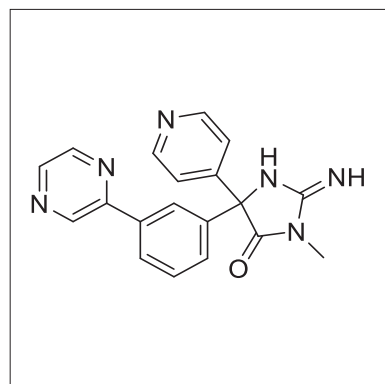
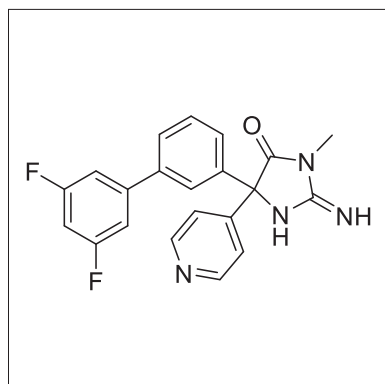


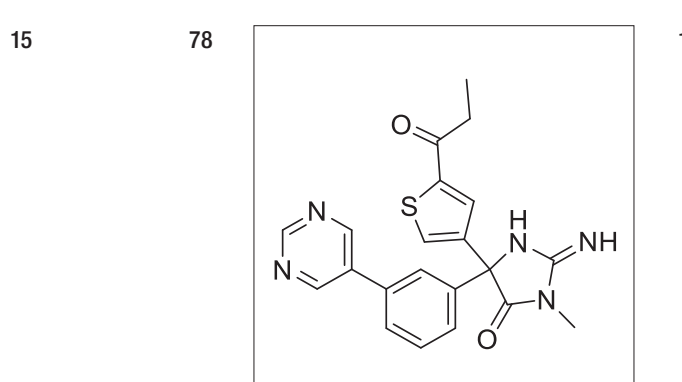
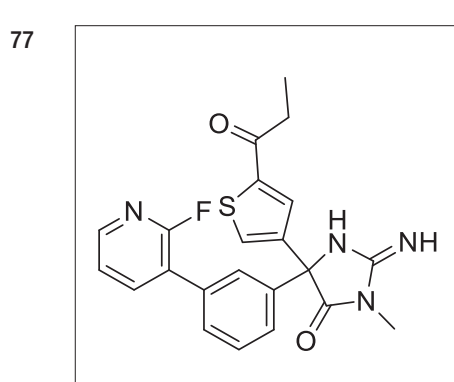
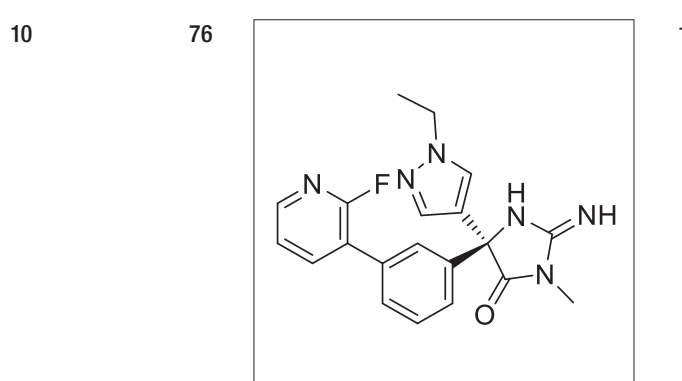
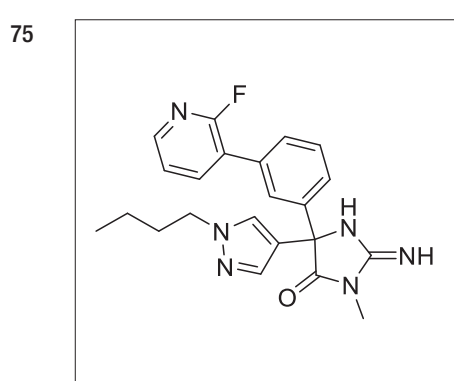
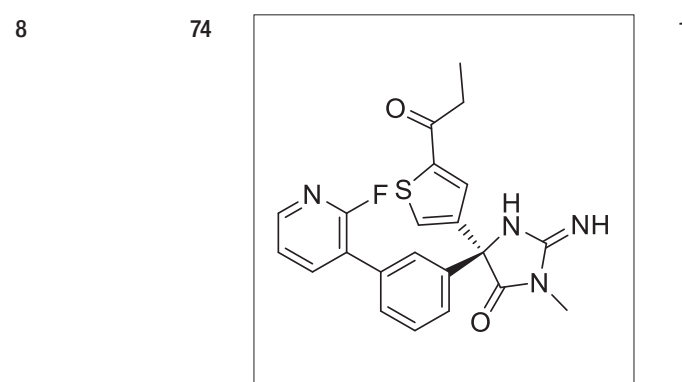
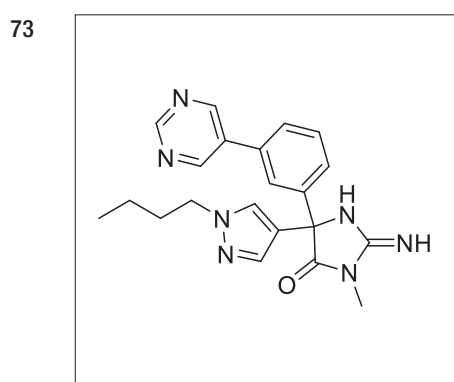
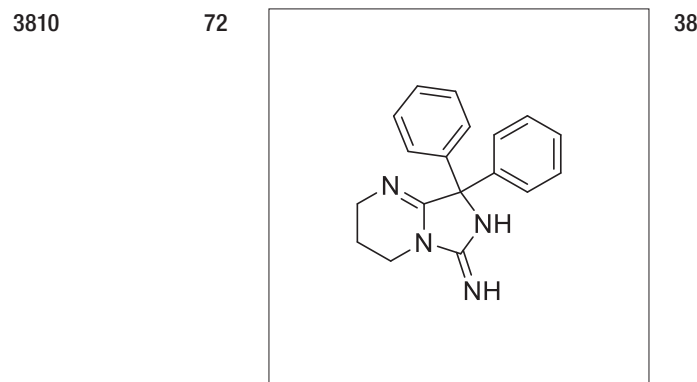
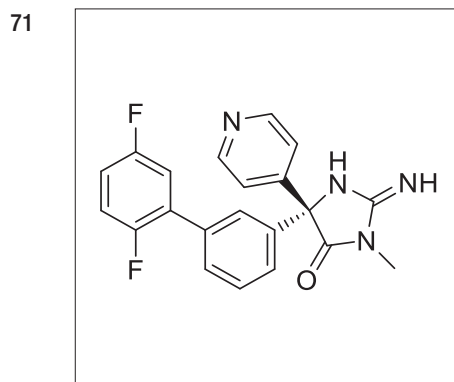
50

62

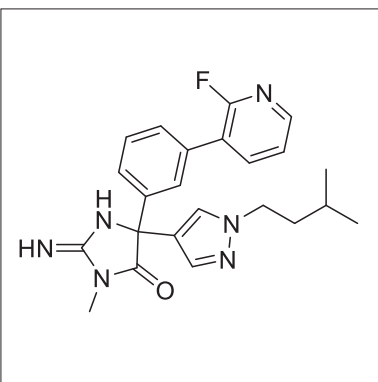


60



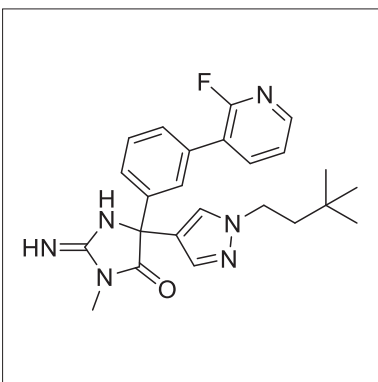


79



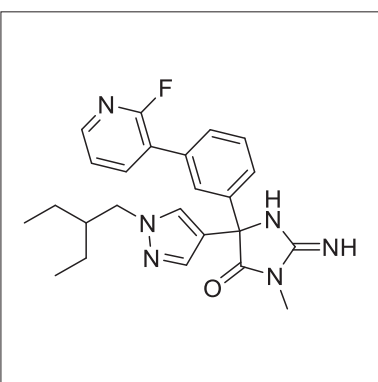
16

80



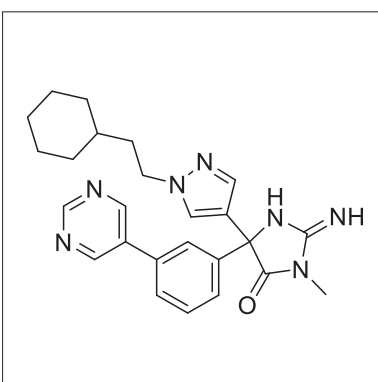
20

81



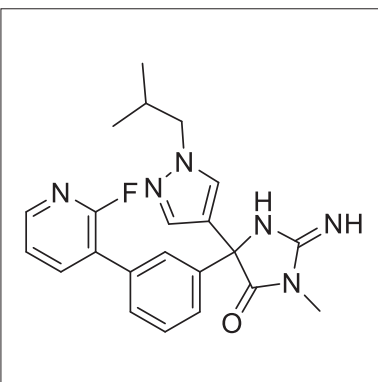
20

82



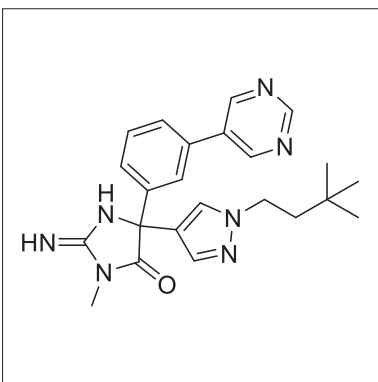
20

83



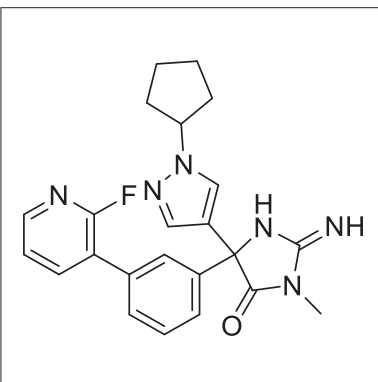
20

84



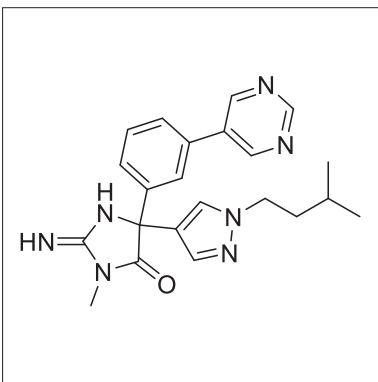
20

85



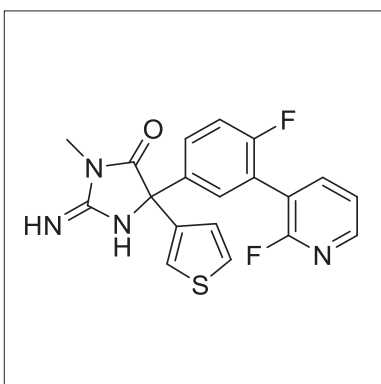
20

86



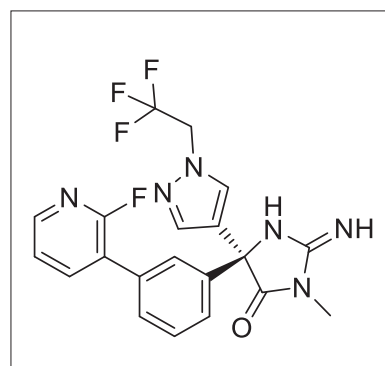
30

87



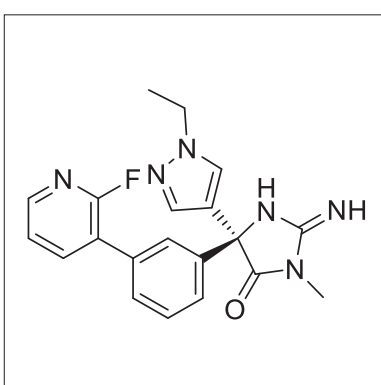
30

88



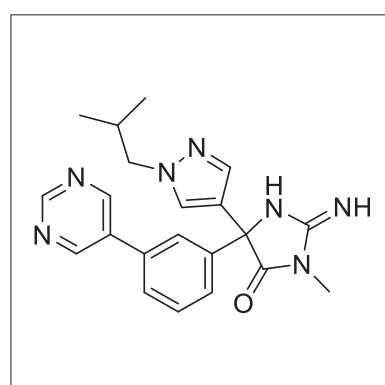
30

89



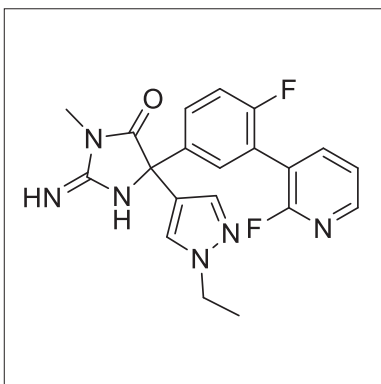
30

90



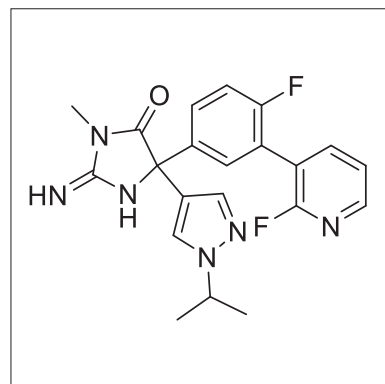
30

91



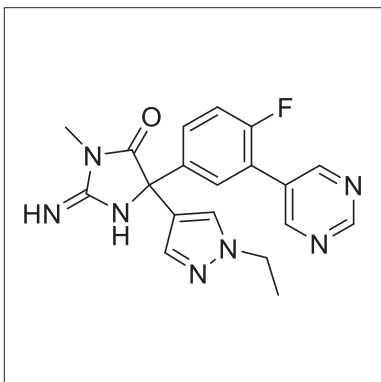
30

92



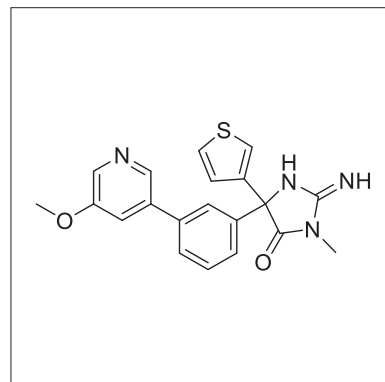
40

93



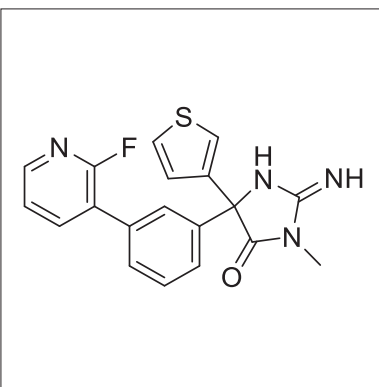
40

94



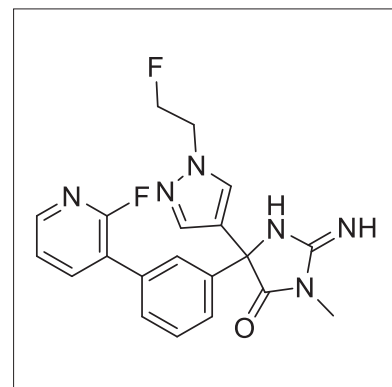
40

95



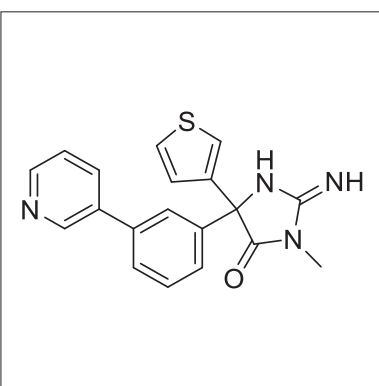
40

96



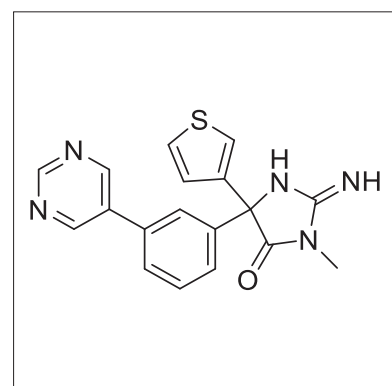
50

97



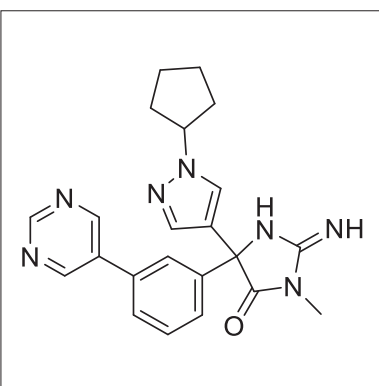
60

98



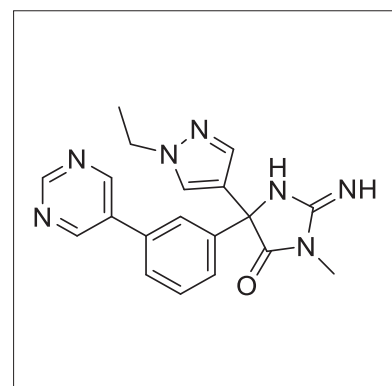
70

99



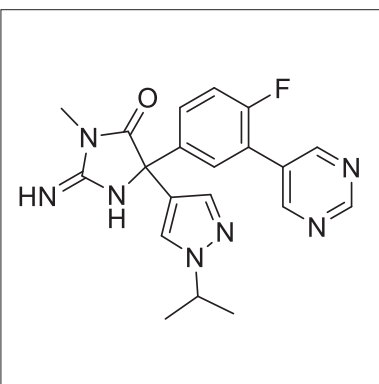
70

100



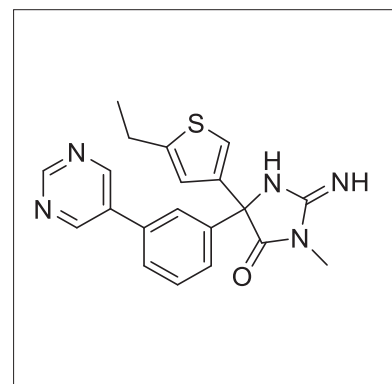
80

101



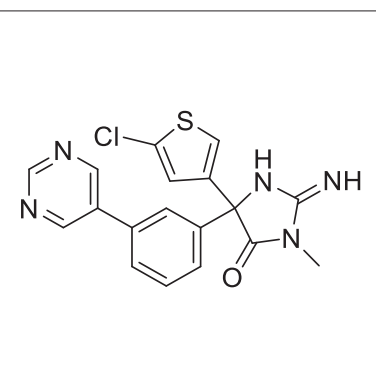
80

102



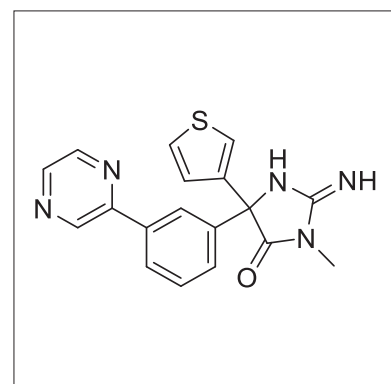
80

103



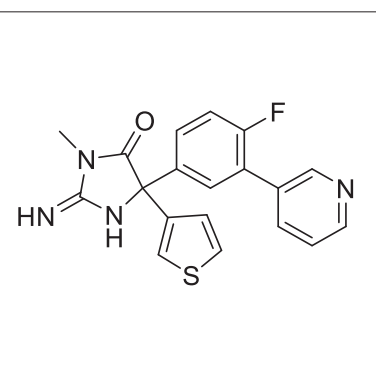
80

104



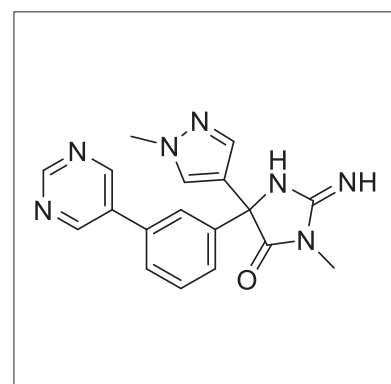
90

105



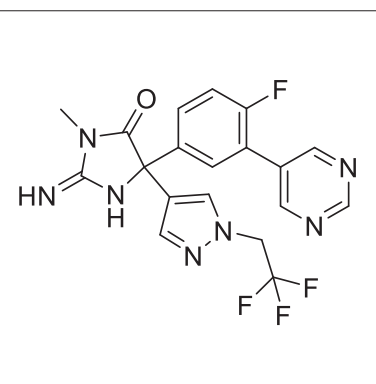
90

106



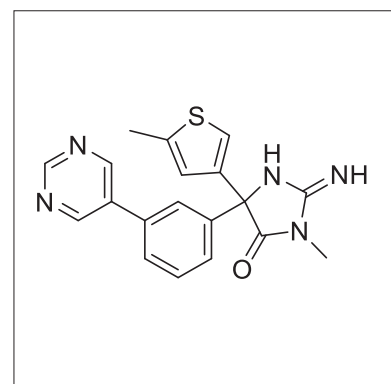
100

107



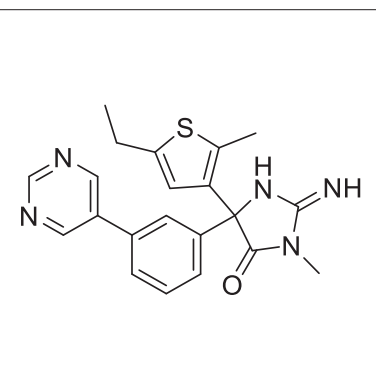
120

108



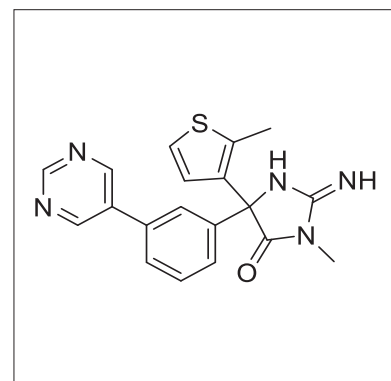
140

109



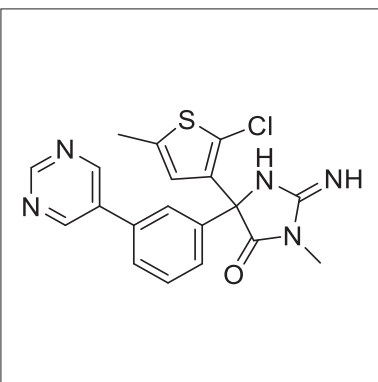
180

110



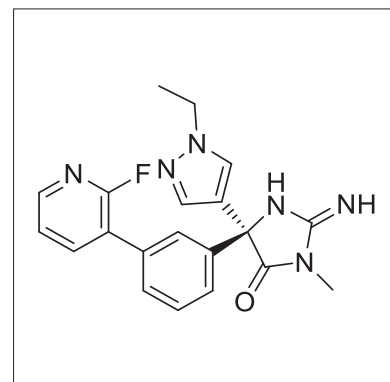
370

111



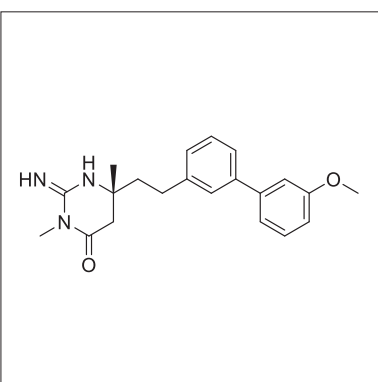
470

112



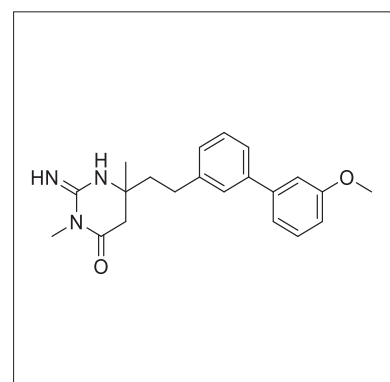
1960

113



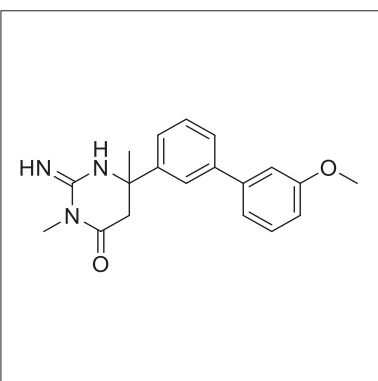
80

114



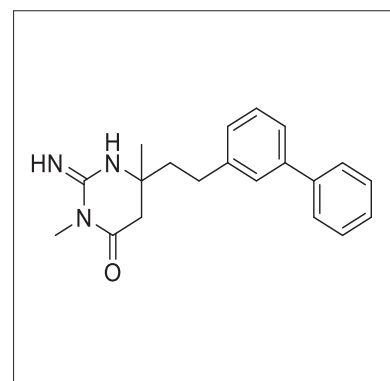
200

115



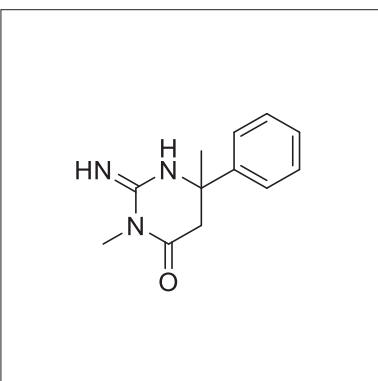
380

116



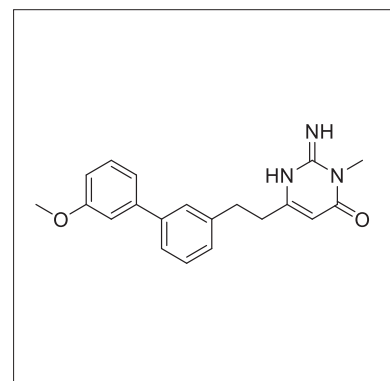
1600

117



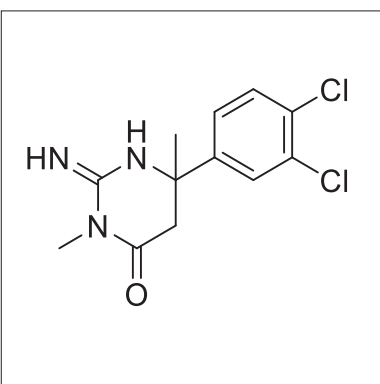
2000

118



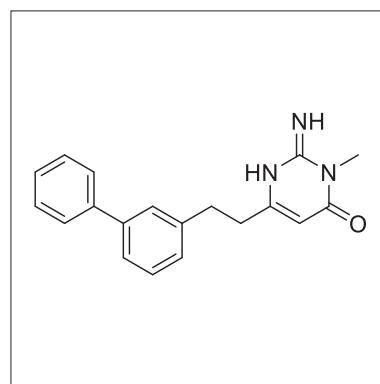
5900

119



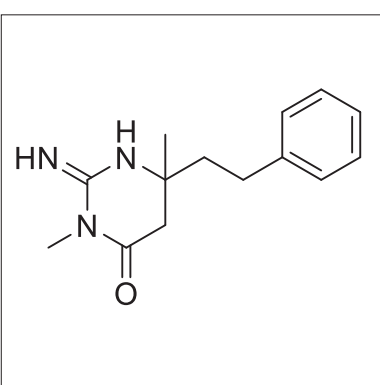
6100

120



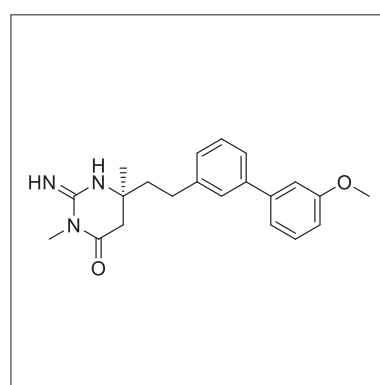
29000

121



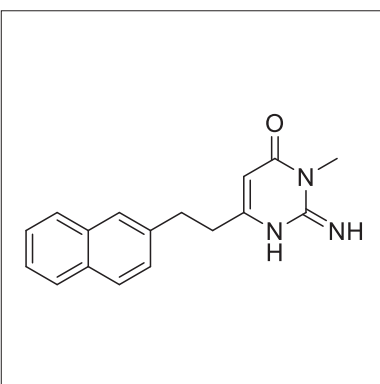
34000

122



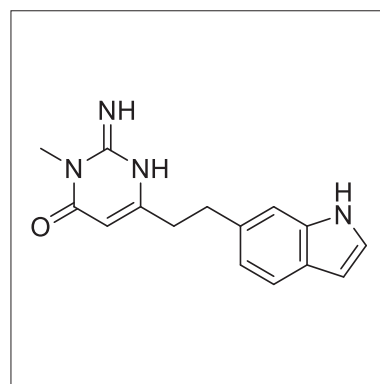
35000

123



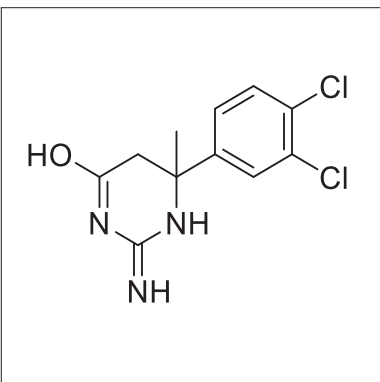
36000

124



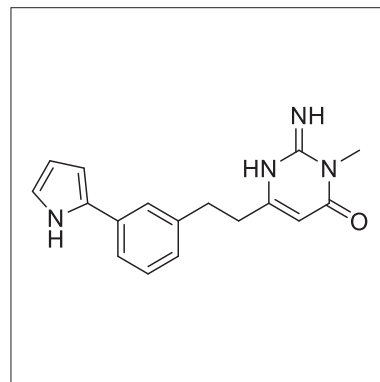
77000

125

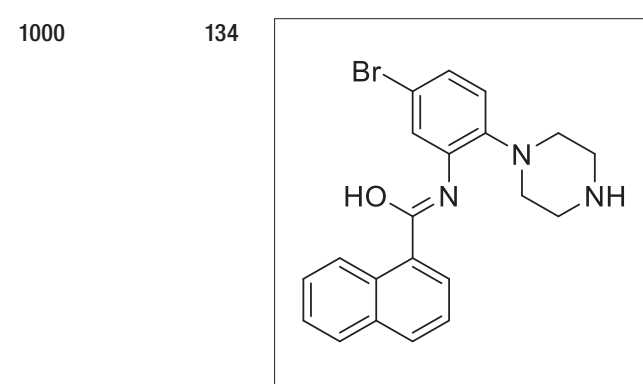
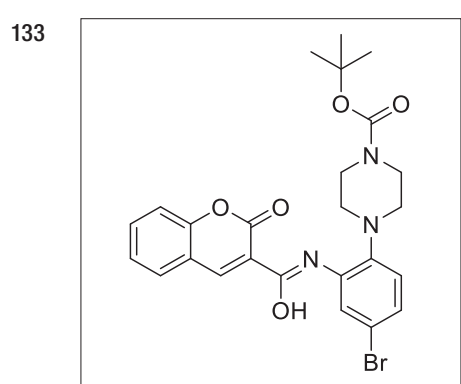
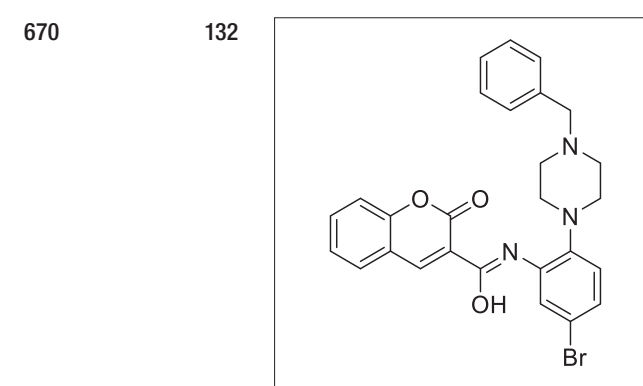
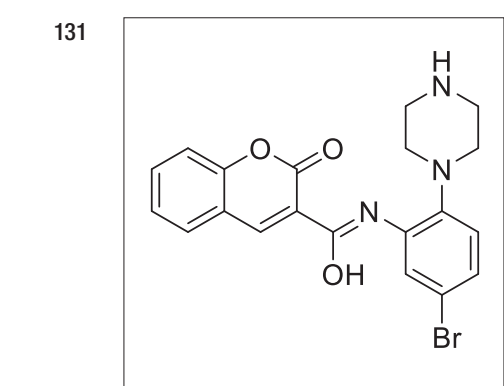
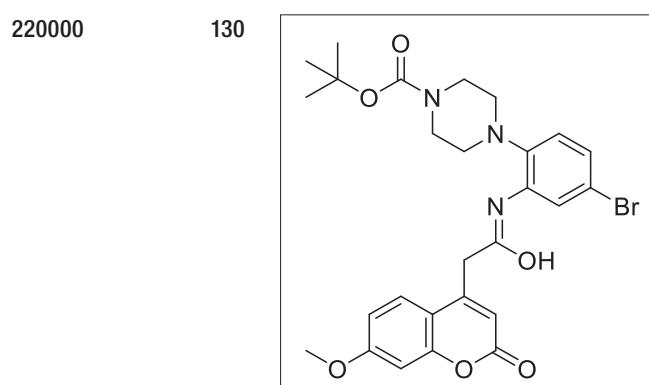
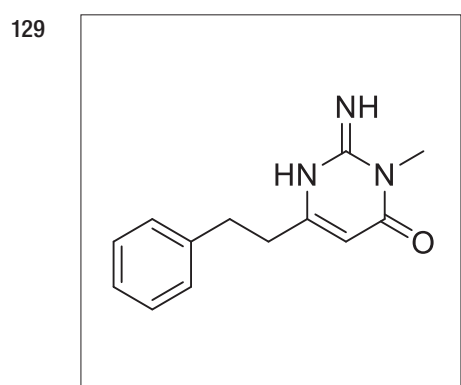
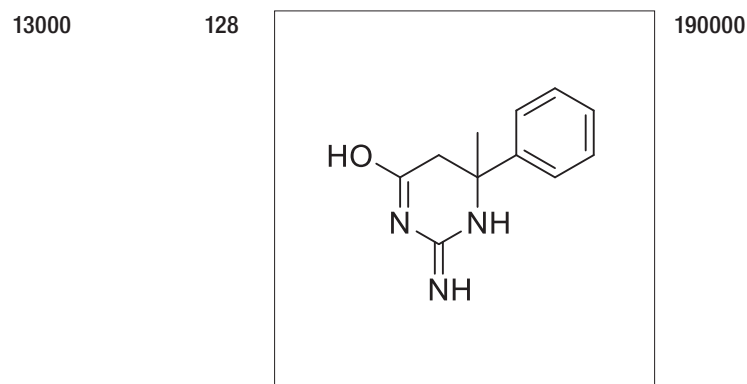
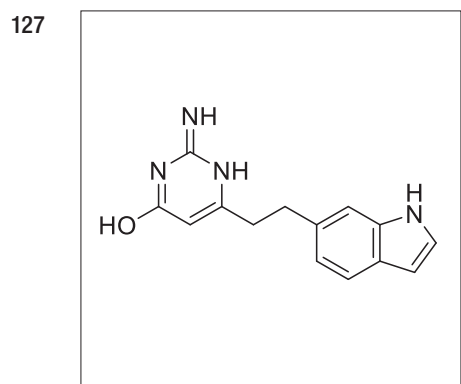


82000

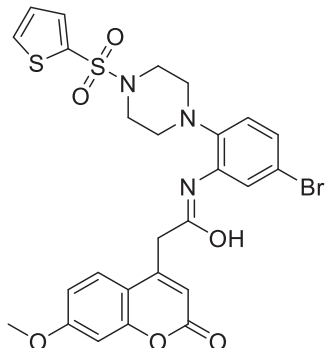
126



99000

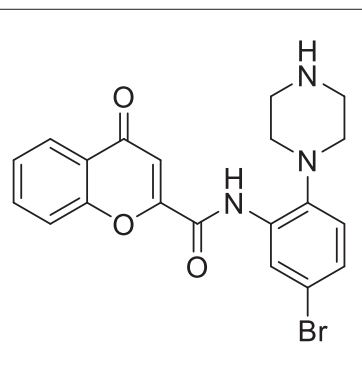


135



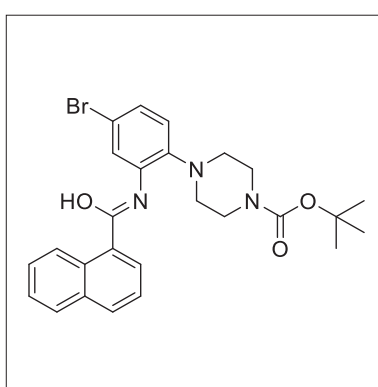
1130

136



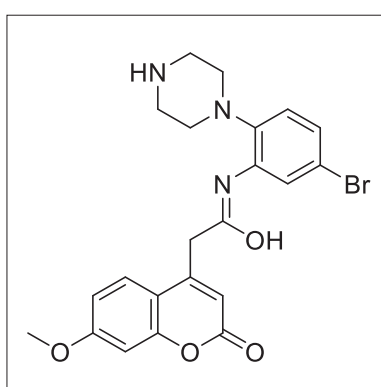
1600

137



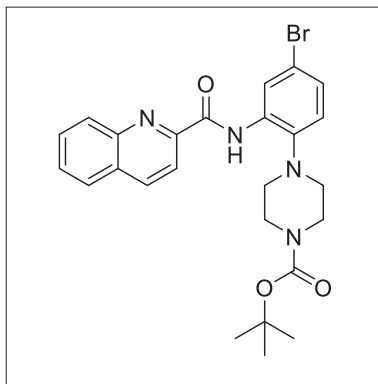
1700

138



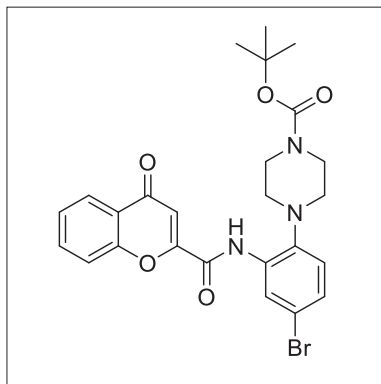
1700

139



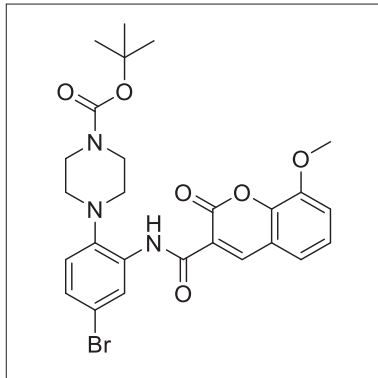
1700

140



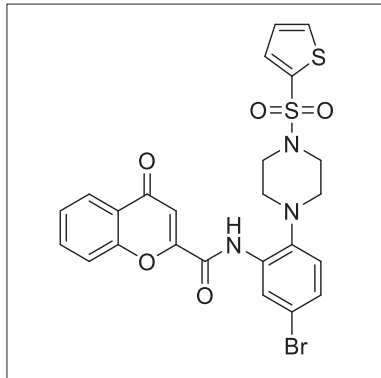
1900

141

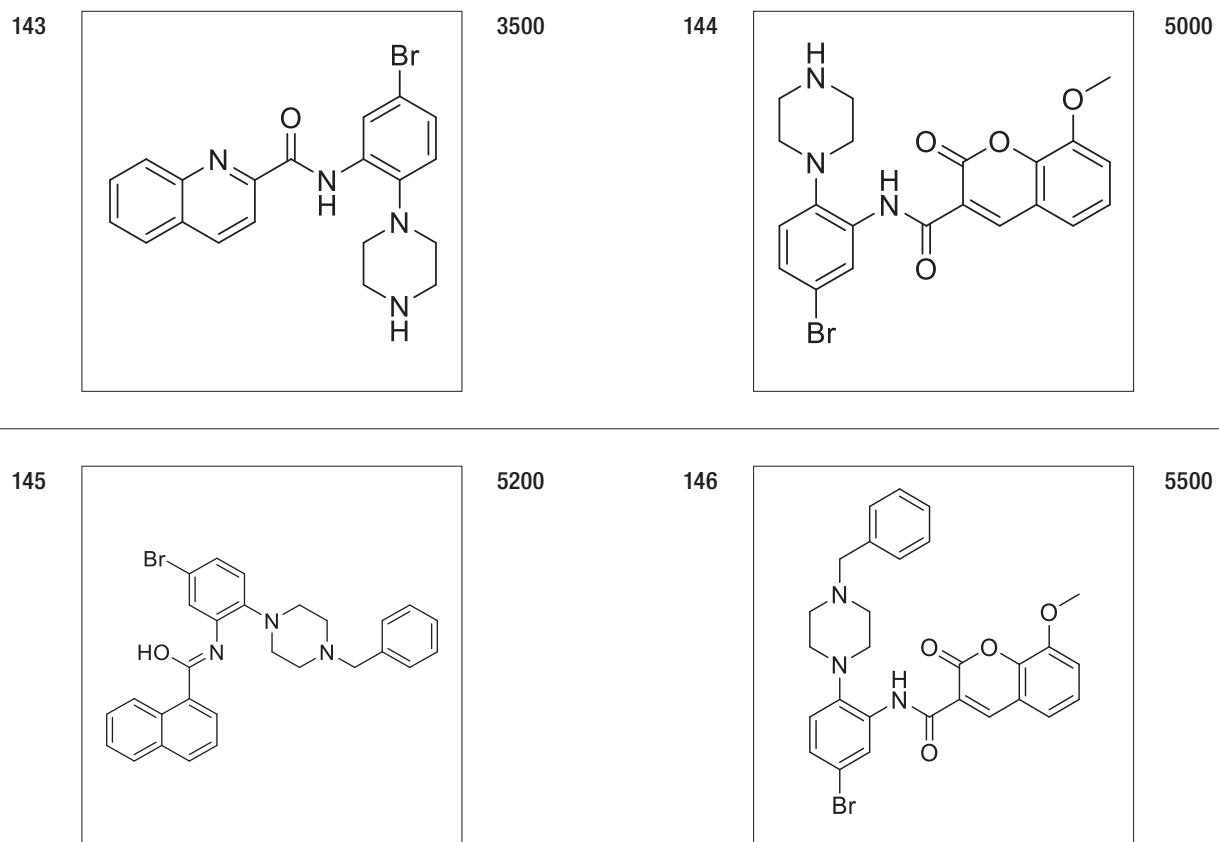


2400

142



2600



SN: serial number;

Alignment procedure

The alignment of molecules is a critical step in the development of 3D-QSAR models (Figure 1). For this study, molecule 73, identified as one of the most active compounds and characterised by its lowest energy conformation, was selected as

the reference structure. All other molecules in the dataset were aligned to this reference molecule to ensure consistency in the 3D spatial arrangement, which is essential for accurate QSAR model generation.

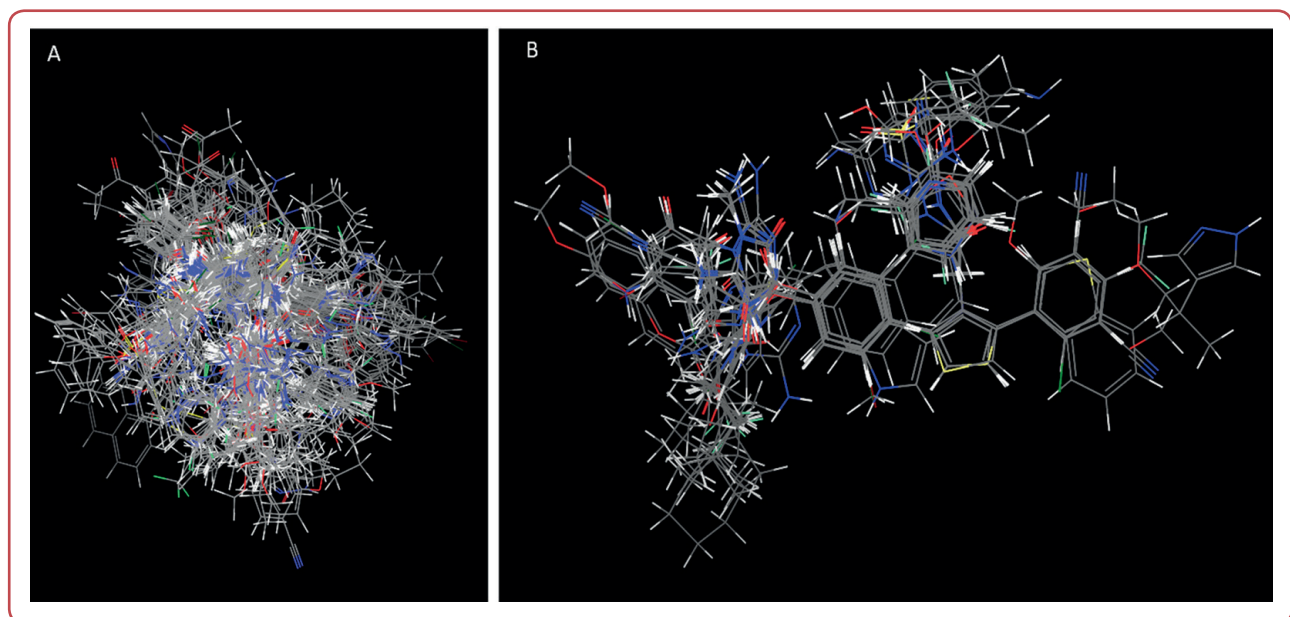


Figure 1: Common core-based alignment using highly active molecule 73; a) Non-aligned molecules; B) Aligned molecules;

Field- and atom-based 3D-QSAR model energy calculations

The 3D-QSAR tool in *Schrödinger Maestro* software was used to perform 3D-QSAR analysis using both field-based and atom-based techniques. The 3D-QSAR technique constructs predictive models by correlating the biological activities of aligned molecules with their 3D structural characteristics. The field-based QSAR model,²⁰ calculates interaction energies based on steric, electrostatic, hydrophobic, hydrogen bond donor (HBD) and hydrogen bond acceptor (HBA) potential fields, utilising Gaussian functions for these calculations. This model is alignment-dependent, meaning that the molecular field interaction energy terms are statistically correlated with biological activities or responses through multivariate analyses. During the construction of field-based models, the steric and electrostatic force fields were constrained to 30.0 kcal/mol.

On the other hand, the atom-based QSAR 22 method depicts every molecule as a group of overlapping van der Waals spheres. Each atom and thus each sphere, is classified according to certain criteria: atoms with a negative ionic charge are classified as negative ionic (N); atoms with a positive ionic charge are classified as positive ionic (P); non-ionic nitrogen and oxygen are classified as electron-withdrawing (W); hydrogens bonded to polar atoms are defined as hydrogen bond donors (D); carbons, halogens and C-H hydrogens are defined as hydrophobic/non-polar (H); and all other atoms are classified as miscellaneous (X). When using atom-based QSAR, the regions of interest are highlighted using color-coded cubes, with blue and red representing different types of interactions.

Partial least square (PLS) analysis

In the PLS regression analysis used to generate the 3D-QSAR models, pIC_{50} values served as the dependent variables, while field and atom intensities were employed as independent variables (descriptors).

Workflow for 3D-QSAR model generation

The generation of 3D-QSAR models requires the proper alignment of all molecules. To achieve this, guanidine analogues were processed to obtain their lowest energy conformations using *LigPrep*. The molecules were aligned based on a highly active reference compound. Ultimately, the lowest energy conformations of 73 molecules

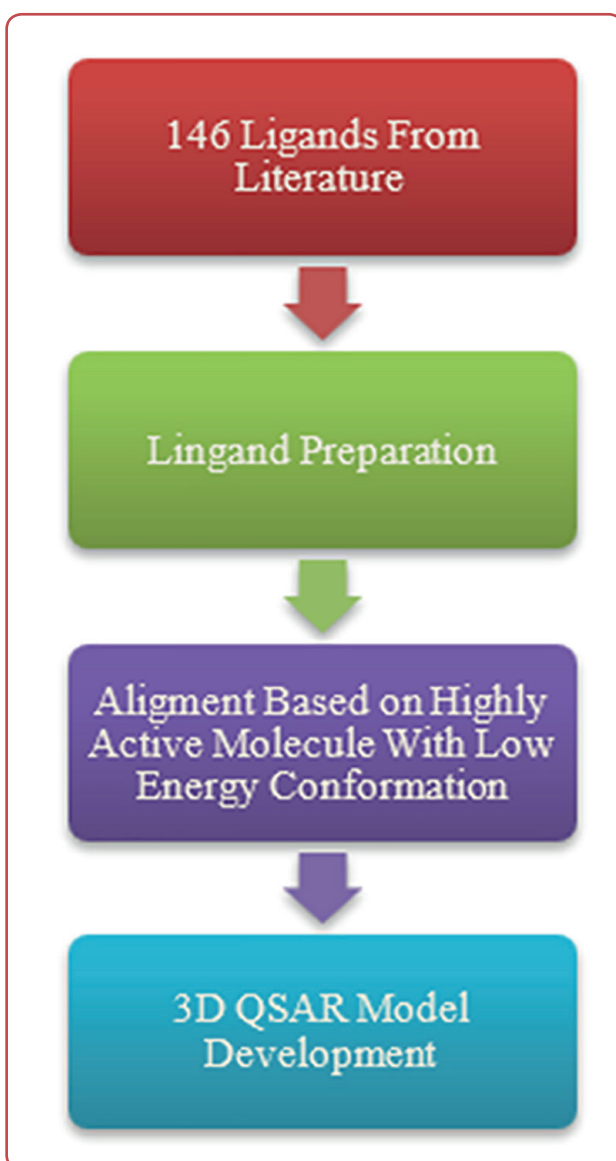


Figure 2: Workflow for 3D-QSAR model generation

were selected for the development of Field- and Atom-based 3D-QSAR models. Figure 2 shows how the 3D-QSAR model generation process is carried out.

Results

3D-QSAR

The 3D-QSAR analysis, encompassing both field-based and atom-based approaches, was conducted on 146 guanidine-containing inhibitors of the BACE-1 enzyme. The biological activities of these 146 compounds are presented in Table 1, with IC_{50} values ranging from 8 to 5500 nM. As indicated in Table 2, the Predicated activity of the

models was assessed by transforming the *in vitro* IC₅₀ values to equivalent pIC₅₀ (-log IC₅₀) values. 3D-QSAR models were created using the PLS approach, with the pIC₅₀ values acting as dependent

variables and the anticipated values acting as independent variables. As shown in Tables 3 and 4, the models' q² values were used to evaluate their predictive power.

Table 2: Experimental and predicted pIC₅₀ values and prediction error for training and test sets

SN	Field based QSAR			Atom based QSAR	
	QSAR Set	Experimental pIC ₅₀	Predicted pIC ₅₀	Prediction error	Predicted activity
1	Training	6.301	6.014	-0.287	6.002
2	Training	6.222	6.020	-0.202	5.971
3	Training	6.222	5.931	-0.291	5.971
4	Training	6.222	5.941	-0.281	5.925
6	Training	6.155	6.054	-0.101	5.984
8	Training	6.097	5.959	-0.138	5.902
9	Training	6.046	5.955	-0.090	5.910
10	Training	6.046	6.017	-0.028	5.994
12	Training	5.959	5.965	0.006	5.956
13	Training	5.921	6.033	0.112	6.083
14	Training	5.921	5.988	0.068	5.884
15	Training	5.886	5.946	0.060	5.882
16	Training	5.886	5.868	-0.018	5.858
17	Training	5.886	5.918	0.031	5.920
20	Training	5.854	5.909	0.055	5.863
21	Training	5.854	5.896	0.042	5.858
23	Training	5.824	5.924	0.100	5.897
24	Training	5.796	6.009	0.213	5.949
25	Training	5.796	5.902	0.106	5.873
27	Training	5.745	6.000	0.255	6.015
28	Training	5.745	5.882	0.138	5.978
29	Training	5.721	5.755	0.034	5.780
30	Training	5.699	5.462	-0.237	5.591
32	Training	5.523	5.468	-0.055	5.591
33	Training	5.456	5.515	0.059	5.570
34	Training	5.432	5.372	-0.060	5.491
35	Training	5.337	5.374	0.037	5.478
36	Training	6.854	6.546	-0.308	6.460
39	Training	6.585	6.480	-0.105	6.457
40	Training	6.553	6.557	0.004	6.489
41	Training	6.229	6.073	-0.157	5.982
43	Training	6.167	5.969	-0.198	5.988
44	Training	6.125	6.084	-0.041	6.093
46	Training	5.812	6.202	0.389	6.052
47	Training	5.810	6.119	0.309	6.053
48	Training	5.724	5.977	0.254	5.882
49	Training	5.432	5.372	-0.060	5.491
50	Training	5.161	5.299	0.137	5.327
51	Training	5.081	5.454	0.373	5.460
54	Training	7.328	7.772	0.444	7.511
56	Training	7.523	7.327	-0.195	7.119
59	Training	7.398	7.373	-0.025	7.206
60	Training	7.301	7.313	0.011	7.108

62	Training	7.222	7.190	-0.032	7.021	-0.201
63	Training	7.222	7.360	0.138	7.103	-0.119
64	Training	7.155	6.921	-0.234	6.830	-0.325
65	Training	6.886	7.265	0.379	7.067	0.181
66	Training	6.620	6.828	0.208	6.531	-0.089
67	Training	6.602	7.002	0.400	7.089	0.486
68	Training	6.201	6.653	0.453	6.575	0.374
69	Training	5.572	5.663	0.091	5.504	-0.068
70	Training	5.444	5.590	0.146	5.364	-0.079
72	Training	4.420	4.899	0.479	4.484	0.064
73	Training	8.097	7.350	-0.747	7.698	-0.399
74	Training	8.000	8.024	0.024	8.209	0.209
75	Training	8.000	7.681	-0.319	7.964	-0.036
77	Training	7.824	7.772	-0.052	7.733	-0.091
78	Training	7.824	7.503	-0.321	7.543	-0.281
79	Training	7.796	7.639	-0.157	7.864	0.068
80	Training	7.699	7.760	0.061	8.003	0.304
81	Training	7.699	7.822	0.123	8.013	0.314
82	Training	7.699	7.474	-0.225	7.754	0.055
84	Training	7.699	7.499	-0.200	7.811	0.113
85	Training	7.699	7.665	-0.034	7.677	-0.022
86	Training	7.523	7.372	-0.151	7.672	0.150
87	Training	7.523	7.363	-0.159	7.275	-0.248
89	Training	7.523	7.386	-0.137	7.362	-0.161
90	Training	7.523	7.327	-0.196	7.435	-0.088
91	Training	7.523	7.466	-0.057	7.403	-0.120
92	Training	7.398	7.418	0.020	7.344	-0.054
93	Training	7.398	7.135	-0.263	7.137	-0.261
94	Training	7.398	7.417	0.019	7.256	-0.142
95	Training	7.398	7.349	-0.049	7.308	-0.090
96	Training	7.301	7.404	0.103	7.399	0.098
98	Training	7.155	7.082	-0.073	7.117	-0.038
99	Training	7.155	7.398	0.243	7.486	0.331
100	Training	7.097	7.120	0.023	7.171	0.074
101	Training	7.097	7.151	0.055	7.153	0.056
102	Training	7.097	7.252	0.155	7.224	0.127
103	Training	7.097	7.155	0.058	7.095	-0.002
106	Training	7.000	7.001	0.001	7.029	0.029
107	Training	6.921	7.080	0.160	7.128	0.207
108	Training	6.854	7.163	0.309	7.104	0.251
109	Training	6.745	7.123	0.378	7.005	0.260
114	Training	6.699	6.195	-0.504	6.188	-0.511
115	Training	6.420	6.743	0.323	6.674	0.254
116	Training	5.796	6.005	0.209	6.117	0.321
117	Training	5.699	4.957	-0.742	5.032	-0.667
118	Training	5.229	4.938	-0.291	4.977	-0.252
121	Training	4.469	4.404	-0.065	4.555	0.087
122	Training	4.456	4.392	-0.064	4.236	-0.220
123	Training	4.444	4.254	-0.189	4.309	-0.135
124	Training	4.114	3.739	-0.375	3.868	-0.245
125	Training	4.086	4.795	0.709	4.736	0.650
126	Training	4.004	4.542	0.537	4.547	0.543
127	Training	3.886	3.762	-0.124	3.910	0.024

129	Training	3.658	3.592	-0.065	3.924	0.266
130	Training	7.032	6.604	-0.428	6.759	-0.272
131	Training	6.174	5.958	-0.216	5.901	-0.273
132	Training	6.119	5.910	-0.209	5.932	-0.188
133	Training	6.000	6.087	0.087	5.988	-0.012
134	Training	6.000	5.822	-0.178	5.874	-0.126
135	Training	5.947	6.282	0.336	6.296	0.349
137	Training	5.770	5.960	0.191	5.956	0.187
139	Training	5.770	5.816	0.047	5.798	0.028
140	Training	5.721	5.609	-0.112	5.707	-0.014
141	Training	5.620	5.639	0.019	5.542	-0.078
142	Training	5.585	5.301	-0.284	5.254	-0.331
144	Training	5.301	5.506	0.205	5.440	0.139
146	Training	5.260	5.463	0.203	5.467	0.207
5	Test	6.222	6.104	-0.118	6.028	-0.194
7	Test	6.155	5.810	-0.345	5.914	-0.240
11	Test	6.000	5.959	-0.041	5.884	-0.116
18	Test	5.886	5.916	0.029	5.834	-0.052
19	Test	5.886	5.999	0.113	5.892	0.006
22	Test	5.854	5.947	0.093	6.023	0.170
26	Test	5.770	5.859	0.090	5.917	0.147
31	Test	5.699	5.509	-0.190	5.570	-0.129
37	Test	6.824	6.139	-0.684	6.084	-0.740
38	Test	6.699	6.416	-0.283	6.347	-0.352
42	Test	6.201	5.454	-0.747	5.458	-0.743
45	Test	6.032	6.590	0.558	6.635	0.604
52	Test	4.222	5.101	0.879	5.729	1.507
53	Test	7.745	6.453	-1.292	6.357	-1.388
55	Test	7.699	7.498	-0.201	7.184	-0.515
57	Test	7.523	7.455	-0.068	7.136	-0.387
58	Test	7.398	7.298	-0.100	7.039	-0.358
61	Test	7.301	7.378	0.077	7.229	-0.072
71	Test	5.419	7.378	1.959	7.229	1.810
76	Test	8.000	7.542	-0.458	7.688	-0.312
83	Test	7.699	7.654	-0.045	7.699	0.001
88	Test	7.523	7.544	0.022	7.624	0.101
97	Test	7.222	7.228	0.007	7.187	-0.035
104	Test	7.046	7.014	-0.032	7.098	0.052
105	Test	7.046	7.244	0.198	7.154	0.108
110	Test	6.432	6.953	0.521	6.898	0.466
111	Test	6.328	6.983	0.655	6.936	0.608
112	Test	5.708	7.386	1.678	7.362	1.655
113	Test	7.097	6.192	-0.905	6.135	-0.962
119	Test	5.215	5.164	-0.051	5.093	-0.121
120	Test	4.538	4.849	0.311	4.946	0.409
128	Test	3.721	4.603	0.881	4.674	0.953
136	Test	5.796	5.479	-0.317	5.620	-0.176
138	Test	5.770	6.479	0.709	6.661	0.891
143	Test	5.456	5.691	0.235	5.711	0.255
145	Test	5.284	5.747	0.463	5.918	0.634

SN: serial number;

Field-based 3D-QSAR model

The initial field-based model was created to evaluate the molecules' steric, electrostatic, hydrophobic, HBD and HBA characteristics related to their anti-Alzheimer action. Table 3 presents the statistical results obtained from this field-based model. Figure 6A illustrates a scatter plot of the field-based model, showing that nearly all molecules fall within the expected range, indicating the model's predictive capability. The steric, electrostatic, HBA, HBD and hydrophobic strengths of the training set corresponded using partial least squares (PLS) regression using six factors to create the field-based 3D-QSAR model. Using the leave-one-out (LOO) cross-validation approach, the model obtained a R^2_{cv} value of 0.7353. The non-cross-validation analysis produced a R^2 value of 0.9428, with a F ratio of 283.1 and a standard error of the value of 0.2505. This model's steric and electrostatic contributions were 0.387 and 0.072, accordingly, suggesting that steric interactions are more important in protein-ligand binding than electrostatic interactions. Table 3 provides specifics on the percentage contributions of the electrostatic and steric field strengths. Expected pIC_{50} values for 36 testing-set inhibitors were computed for model validation. The model appears to have a reasonably high predictive capacity, as shown

Table 3: Partial least squares (PLS) regression using data summary on the percentage contributions of the electrostatic and steric field strengths

Statistical parameters	Field-based QSAR
SD	0.2505
R^2	0.9428
R^2_{cv}	0.7353
R^2 scramble	0.4028
Q^2	0.6155
Stability	0.8400
F	283.100
P	1.23E-61
RMSE	0.6300
Pearson-r	0.7925
Filed contributions	
Gaussian steric	0.387
Gaussian electrostatic	0.072
Gaussian hydrophobic	0.254
Gaussian H-bond acceptor	0.180
Gaussian H-bond donor	0.107

SD: standard deviation; RMSE: root mean squared error;

by the predictive correlation coefficient (Q^2) of 0.6155.). Field-based QSAR model generated contour maps are showed in Figure 3A-E.

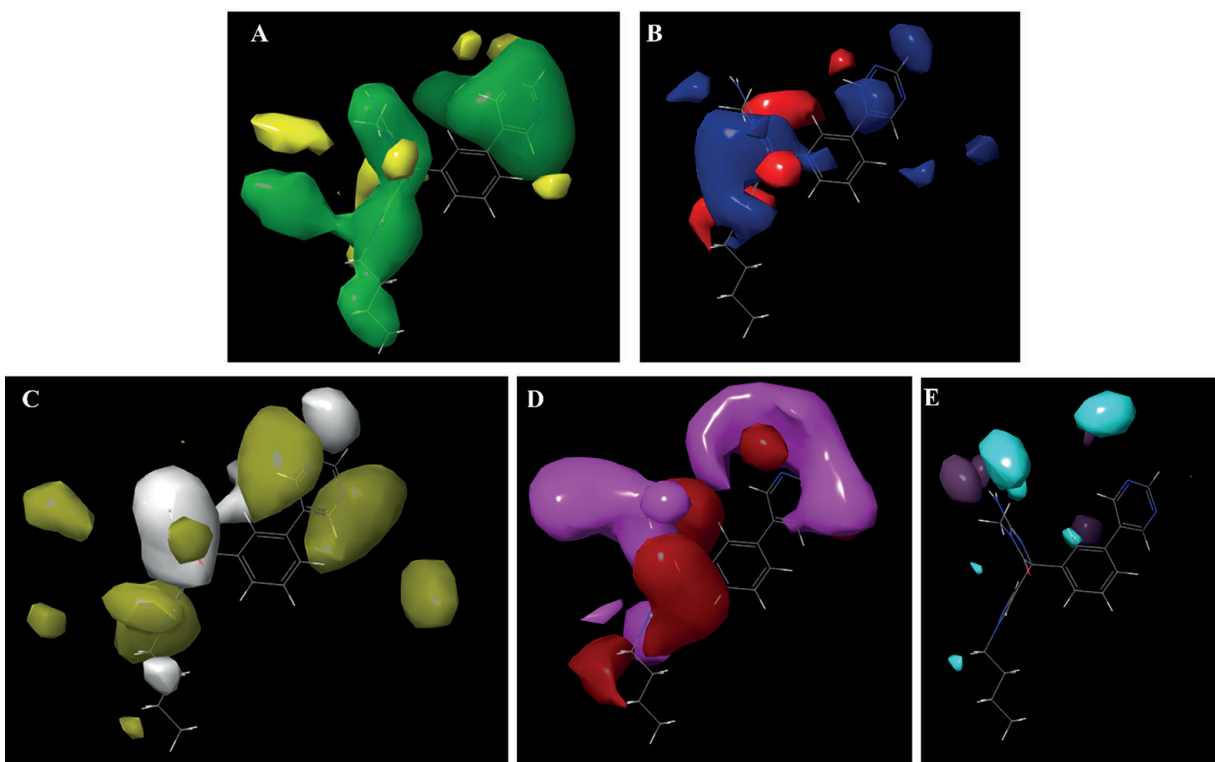


Figure 3: Contour maps obtained for the best Gaussian based 3D QSAR model; A. Steric; B. Electrostatic; C. Hydrophobic; D. Hydrogen bond acceptor; E. Hydrogen bond donor;

Atom-based 3D QSAR model

Using PLS regression with six factors, an atom-based QSAR model was developed by correlating the biological activity with three key fields: hydrophobicity, hydrogen bond donor (HBD) and electron-withdrawing properties. The model obtained an R^2_{cv} value of 0.764 using the leave-one-out (LOO) cross-validation method. The non-cross-validated examination produced an R^2 value of 0.9516, a standard error of estimate of 0.2306 and an F ratio of 337.2, indicating a strong model. Table 4 presents the statistical analysis of the model. The contributions of the hydrophobic, HBD and electron-withdrawing fields were 0.678, 0.051 and 0.238, respectively.

Table 4: Partial least squares (PLS) data summary of the contributions of the six distinct field intensities

Statistical parameters	Field-based QSAR
SD	0.2306
R^2	0.9516
R^2_{cv}	0.7640
$R^2_{scramble}$	0.5123
Q^2	0.5551
Stability	0.8530
F	337.20
P	2.48E-65
RMSE	0.6800
Pearson-r	0.7519
Field contribution	
Gaussian hydrophobic/ non-polar	0.678
Electron withdrawing	0.238
Gaussian H-bond donor	0.051
Other	0.033

SD: standard deviation; RMSE: root mean squared error;

The higher contribution of the hydrophobic field (0.678) relative to the electron-withdrawing and HBD fields suggests that hydrophobic interactions are more critical for protein-ligand binding in this context. The field-based QSAR model provided similar contributions to the produced model. Table 1 shows the predicted IC_{50} values for the compounds, while Table 4 describes the contributions of the six distinct field intensities. Atom-based QSAR model generated contour maps are shown in figure 4A-C.

Validation of field- and atom-based 3D-QSAR models

Figures 5A-B show predicted versus true binding affinities for the training and test set inhibitors, corresponding to the field- and atom-based 3D QSAR models.

Structure activity relationship (SAR)

The field- and atom-based QSAR analysis provided robust statistical data to elucidate the structure-activity relationship (SAR). This SAR study consists of four components (Figure 6): the first part is a ring bridge connected to the second part, which contains a heterocyclic ring; the other end is connected to the third part, a cyclic or open-chain guanidine or its bioisostere residue, which is further extended by the fourth part, a ring or open-chain fragment. Sterically and electrostatically favoured regions were identified on both sides of the bridge, with a higher HBA (hydrogen bond acceptor) to HBD (hydrogen bond donor) ratio, favouring HBA. The hydrophobic region indicates that optimal lipophilicity, necessary for activity, shifts towards the hydrophobic region.

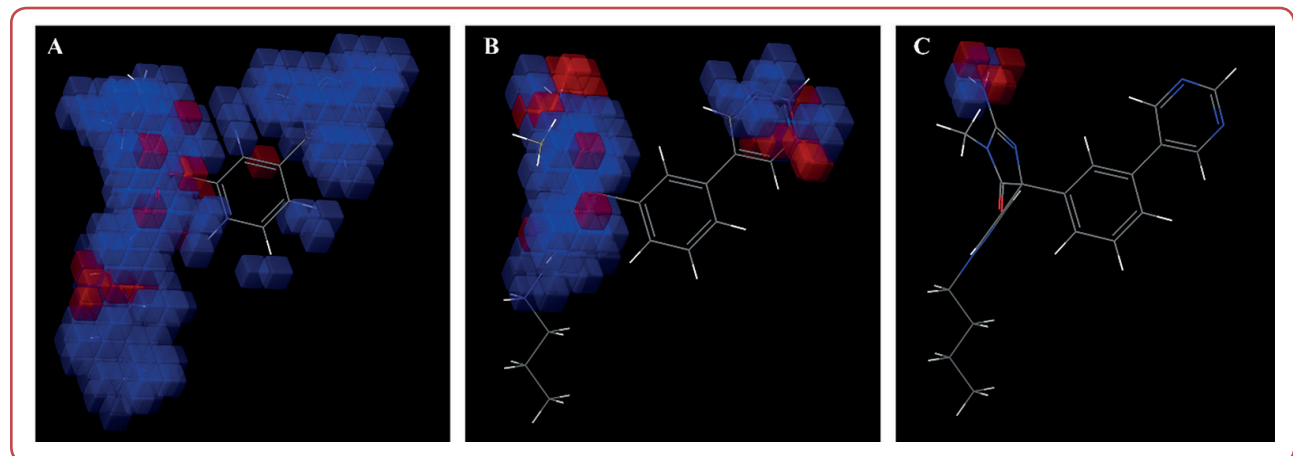


Figure 4: Graphical representation of contours generated using the three-dimensional QSAR model on the most active compound (compound 73). Blue cubes represent favourable regions for the activity; red cubes represent unfavourable regions for the activity. A. Hydrophobic/non-polar; B. Electron withdrawing; C. Hydrogen bond donor;

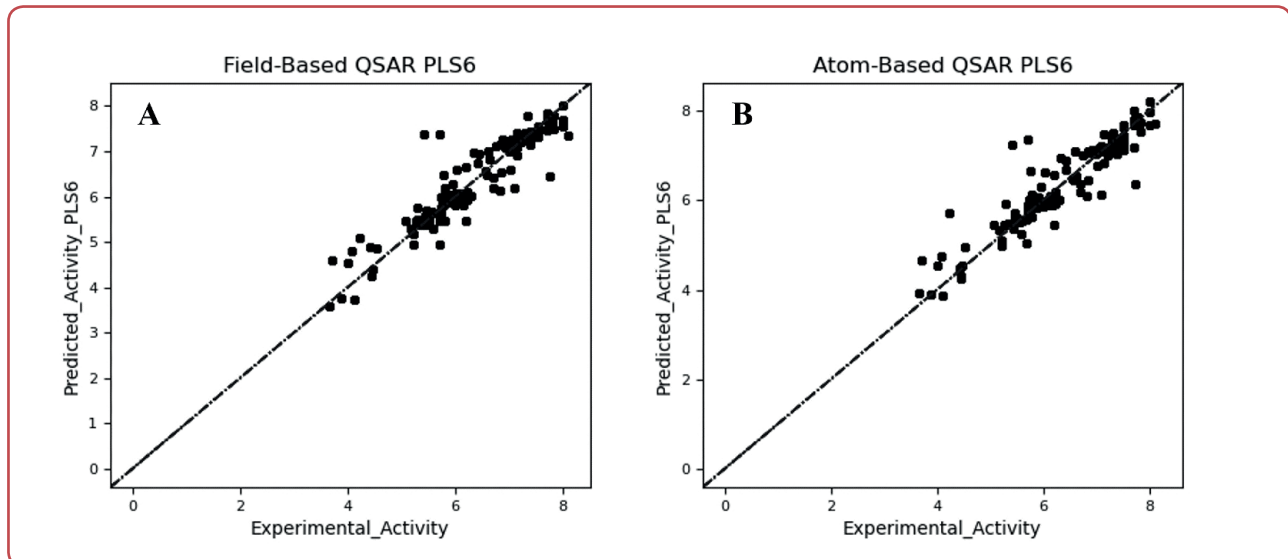


Figure 5: Scatter plots of A) field- and B) atom-based 3D QSAR model

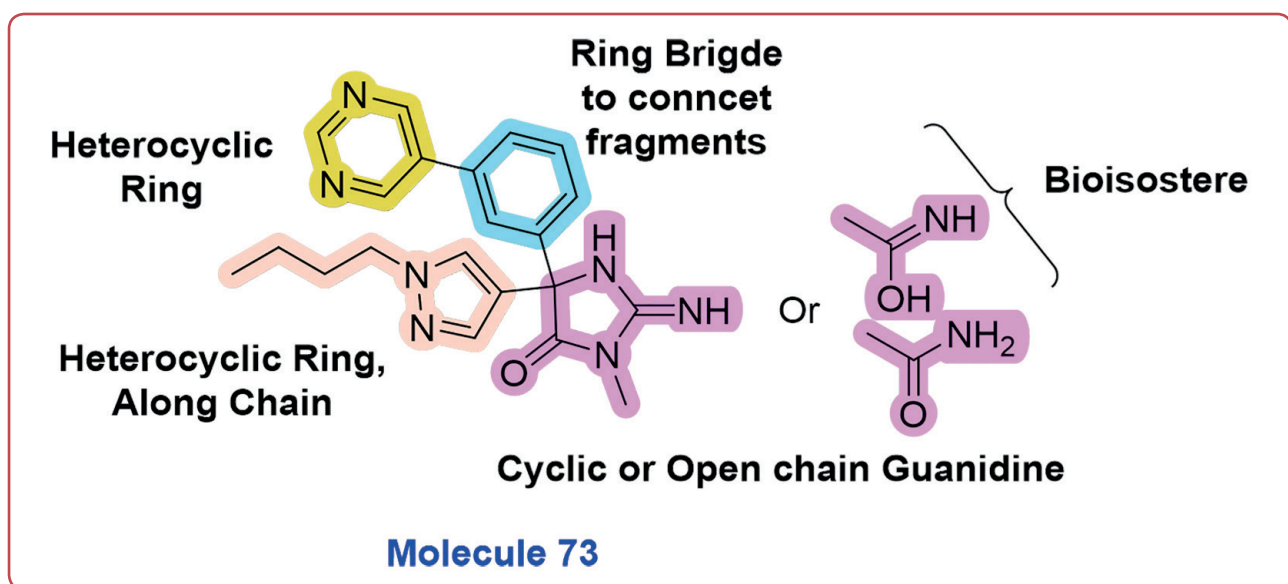


Figure 6: SAR based on 3D-QSAR models like Field and Atom-based QSAR

In consideration of the information acquired so far, novel molecules have been developed (Table 5) and their pIC_{50} values have been predicted with the aid of field and atom-based QSAR models. Further molecular docking studies (MOE 2022.02) supported to claim its BACE-1 inhibitory potency (Table 6 and Figure 7). The designed molecules feature a heterocyclic core structure, with a fused ring bridge connected to an additional fragment, enhancing their structural complexity and potential biological activity. A key modification in these molecules is the replacement of the guanidine fragment with bioisosteric groups, which are designed to maintain or improve the pharmacological properties of the original scaf-

fold. Additionally, it optimises pharmacokinetic properties, particularly in alignment with AD-MET predictions. Notably, the blood-brain barrier (BBB) permeability report suggests that this modification may enhance the molecule's ability to cross the BBB, making it more suitable for central nervous system (CNS) applications. Additionally, the bioisosteric replacement is assumed to retain the biological activity of the original guanidine-containing structure, ensuring that the therapeutic potential of the designed molecules remains intact while potentially improving their drug-like properties. These two series of molecules demonstrated strong predictive performance against the 3D-QSAR models. Among

them, the quinolinone series was found to be more active than the flavonoid series. After summarising the predictions from all QSAR methods, it was discovered that two bulky groups, divided by a nitrogen-containing ring and an alkyl spacer, have significant impacts on BACE-1 inhibitory potency.

The molecular docking study highlights the strong binding potential of the designed molecules, which interacts effectively with key residues of β -secretase, suggesting its potential as a promising inhibitor.

Table 5: Predicted activities of designed molecules by using field and atom based analysis

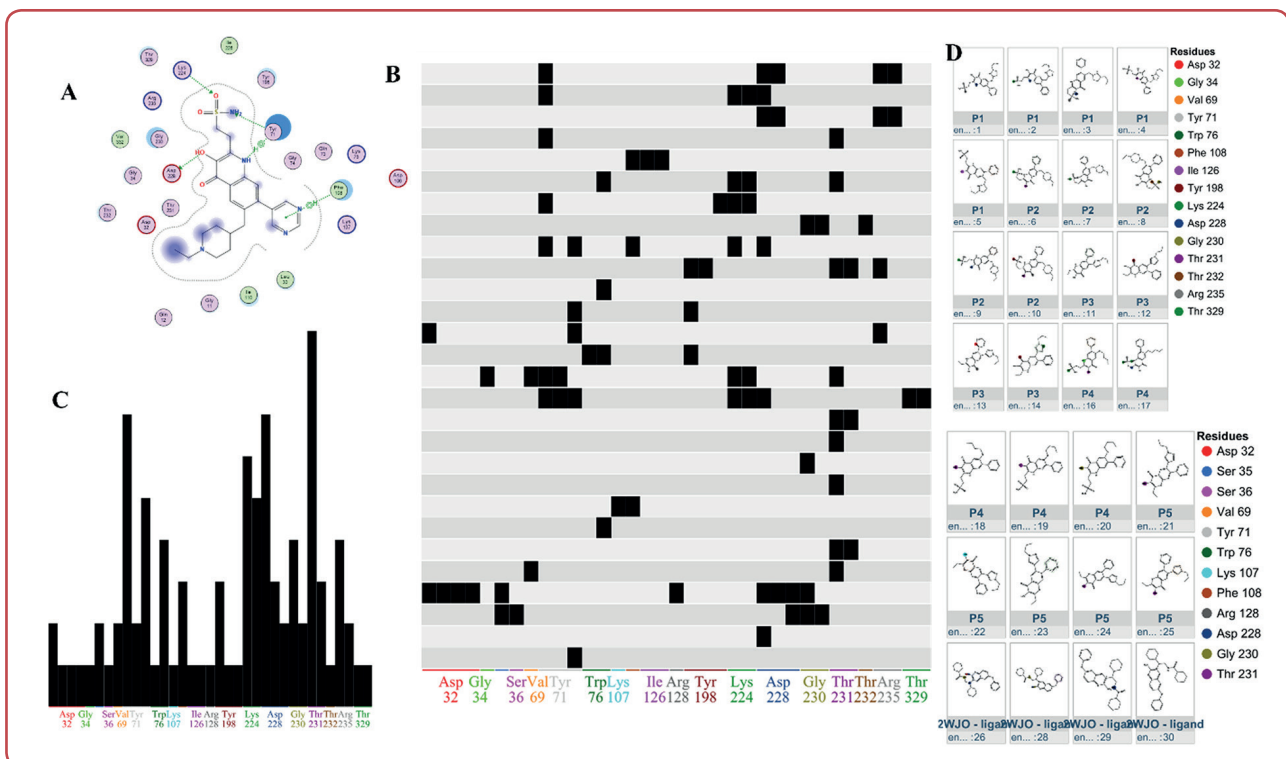


Figure 7: Molecular docking results; A. 2D representation of P2 binding within the β -secretase active site; B. Barcode visualisation of amino acid interaction fingerprints; C. Population distribution of the barcode fingerprint; D. Generated PLIF depicting key residues and their interactions;

Figure 8 presents an ADMET plot as a two-dimensional chart showing the relationship between ADMET_PSA_2D and ADMET_AlogP98. The plot includes two sets of ellipses representing the 95 % and 99 % prediction confidence spaces for the blood-brain barrier penetration (BBB) and human intestinal absorption (HIA) models. Importantly, the predicted compounds P3 and P5 fall within the same ellipse as donepezil, suggesting a similar predictive profile. The other three compounds are located in the outermost ellipse, aligning with the confidence space associated with the QUD-2WJO β -secretase inhibitor.

The molecular docking study of the designed molecules (P1-P5) and the active site ligand (QUD-2WJO) with the target enzyme β -secretase (PDB ID: 2WJO) was conducted to evaluate their binding affinities and interactions within the enzyme's active site. The docking scores, as presented in Table 6, indicate that two of the designed molecules exhibited better binding scores than the QUD ligand. Figure 7 provides a detailed 2D representation of protein-ligand interactions, highlighting the key active site interactions. Additionally, the protein-ligand interaction profiler (PLIP) identified critical amino acid residues in

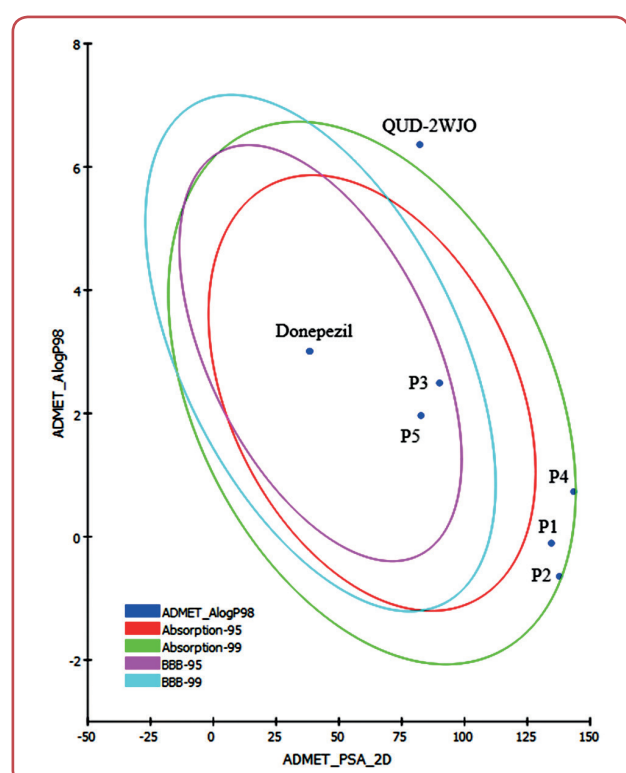


Figure 8: ADMET plot for predicted molecules

volved in these interactions. Among the designed molecules, P2 demonstrated significant interactions with β -secretase, forming hydrogen bonds and hydrophobic interactions with key residues in the active site. Specifically, P2 interacted with ASP 228 (A) at a distance of 2.60 Å with a binding energy of -1.2 kcal/mol, LYS 224 (A) at 3.44 Å with -0.8 kcal/mol, TYR 71 (A) at 3.06 Å with -1.0 kcal/mol and at 3.76 Å with -0.5 kcal/mol and PHE 108 (A) at 3.96 Å with -0.5 kcal/mol. These interactions suggest that designed molecules form stable binding interactions with key residues in the active site of β -secretase, potentially contributing to its inhibitory activity.

Table 6: Docking-derived parameters of the designed derivatives within the binding site of β -secretase

mseq	S	rmsd_refine	E_conf	E_refine
P1	-7.62	2.04	-23.19	-17.64
P2	-7.73	1.74	-26.59	-22.85
P3	-6.27	1.07	62.42	-18.84
P4	-7.40	2.00	-38.85	-25.54
P5	-6.84	1.04	63.60	-22.32
QUD-2WJO	-7.57	1.35	-42.80	-17.15

S, the score of placements of a compound into binding pocket of protein using London dG scoring function, rmsd_refine, the root-mean-squared-deviation (RMSD) between the heavy atoms of the predicted pose (after refinement) and those of the crystal structure (before refinement), E_conf, conformer energy in kcal/mol, E_refine, the score of refinement step of ligand conformer.

Discussion

In the field-based QSAR model, steric interactions are visualised through green and yellow regions. Green regions signify areas where the introduction of bulky substituents is likely to enhance the compound's biological activity. In contrast, yellow regions indicate that bulky substituents in these areas could diminish the activity. In Figure 3A, for the highly active molecule (73), green contours are observed near the pyrimidine and imidazole rings, suggesting that the addition of bulky groups at these sites could potentially increase the compound's activity against the target. In contrast, the presence of a yellow contour close to the imidazole ring's oxygen atom indicates that the addition of bulky substituents in this area

may result in a reduction in biological activity. Figure 3B shows the electrostatic interactions in the field-based QSAR model, which are denoted by red and blue regions. Blue regions indicate areas where the incorporation of electropositive groups could increase the compound's activity, while red regions indicate areas where electronegative groups could improve activity. A prominent red contour near the imidazole ring's oxygen atom indicates that electronegative atoms in this spot are likely to improve activity. Furthermore, blue contours associated with the pyrimidine and pyrazole rings indicate that the presence of electropositive groups in these regions could also contribute positively to the compound's biological activity. In Figure 3C, hydrophobic interactions are illustrated by grey and yellow contours in the hydrophobic plot. Grey areas are where hydrophobic groups are not favoured, so introducing them here might decrease activity. Yellow areas are where hydrophobic groups are accommodated and expected to enhance the biological activity of the compound. Specifically, grey contours around the CH₃ group near the pyrazole and imidazole rings denote unfavourable regions for hydrophobic interactions, while yellow contours on the pyrimidine and pyrazole rings suggest that hydrophobic groups in these areas are more favourable and could enhance the activity. The hydrogen bond acceptor (HBA) contour maps are shown in Figure 3D. Red contours in this map pinpoint certain regions in the molecule in which the presence of HBA groups is favourable to increasing the compound activity. Whereas magenta highlights regions in the molecule where HBA groups may be well accommodated; however, the presence of such group in those areas could potentially reduce the activity of the molecule. A red contour near the pyrazole ring implies that incorporating HBA groups in this subunit could lead to increased activity. In contrast, magenta contours around the pyrimidine and imidazole rings suggest that HBA groups in these positions could potentially diminish the activity. Finally, Figure 3E displays the hydrogen bond donor (HBD) contours, where areas favourable for HBDs are shown in cyan and regions where HBDs are unfavourable are depicted in purple. The cyan region near the benzene ring indicates that introducing HBDs in this area could be beneficial for the compound's activity. Conversely, the purple contour near the imidazole ring suggests that the presence of HBDs in this region might be detrimental to the compound's biological activity.

Atom-based 3D QSAR model, Figure 4A displays the hydrophobic contour maps, where the blue cubes represent regions where hydrophobic groups are favourable for enhancing biological activity. Conversely, the red cubes indicate regions where hydrophobic groups are unfavourable and may reduce activity. Notably, the blue cubes located on the pyrimidine ring and the amino group of the imidazole ring suggest that the presence of hydrophobic substituents in these areas is likely to be beneficial for activity. In contrast, the red cube near the benzene ring indicates that hydrophobic groups in this region may negatively impact activity. Figure 4B illustrates the electron-withdrawing contour maps. The blue cubes in this figure indicate regions where electron-withdrawing groups, acting as hydrogen bond acceptors (HBA), are favourable for biological activity. The red cubes, on the other hand, mark regions where such groups are unfavourable. Specifically, a blue cube on the pyrazole and imidazole rings suggests that electron-withdrawing groups at these positions could enhance activity. In contrast, the red cubes on the pyrimidine ring and the amino group of the imidazole ring indicate that electron-withdrawing groups in these regions may reduce activity. Figure 4C presents the hydrogen bond donor (HBD) contour maps. Blue cubes in this figure highlight regions where HBD groups are favourable for biological activity. Conversely, red cubes represent areas where HBD groups are unfavourable and could decrease activity. A blue cube on the amino group of the imidazole ring suggests that the presence of an HBD group in this location is advantageous for activity. In contrast, the red cubes on the same amino group of the imidazole ring indicate that HBD groups in these regions may be detrimental to activity.

The predicted correlation coefficients (r^2) for the field-based model are 0.9428 and 0.9516, respectively, indicating the atom-based model provides better predictive accuracy. A comparison of the experimentally observed and predicted IC_{50} values for β -secretase inhibitors further demonstrates that the atom-based model excels in predicting the activities of both training and test molecules. Based on the analysis of the statistical parameters for the best field and atom-based 3D-QSAR models, in conclusion, both models have good prediction ability and can provide some knowledge into the chemical properties of the ligands, which may be detrimental to inhibitory processes against β secretase.

Conclusion

In this investigation, a 3D-QSAR study was conducted on selected guanidine (or bioisostere) derivatives. A total of 146 molecules were collected and prepared for the study. The first step involved aligning the dataset molecules after energy minimisation, using the highly active and lowest energy conformation of molecule 73 as a reference to align all other molecules in the series. The molecules were then divided into a training set and a test set in a 75:25 ratio. Field- and atom-based QSAR studies were performed and the scatter plots showed a strong correlation between experimental and predicted pIC_{50} values, indicating good predictive power for the dataset.

The contour plot analysis helped in understanding the structural features required for biological activity. The common structure consisted of four parts: the first part is a ring bridge connected to the second part, which contains a heterocyclic ring; the other end is connected to the third part, a cyclic or open-chain guanidine residue, which is extended by the fourth part, a ring or open-chain fragment. The regions around the bridge exhibited sterically and electrostatically favourable characteristics, with a higher ratio of HBA to HBD, favouring HBA. The hydrophobic region indicated that optimal lipophilicity, necessary for activity, shifted towards the hydrophobic region.

Using the leave-one-out (LOO) cross-validation method, the PLS analysis for the atom-based QSAR model produced an R^2_{cv} value of 0.764, a non-cross-validated R^2 value of 0.9516, a standard error of estimate of 0.2306 and an F ratio of 337.2. According to the PLS analysis, the non-cross-validated R^2 value was 0.9428, with a standard error of estimate of 0.2505, an F ratio of 283.1 and an R^2_{cv} value of 0.7353 for the field-based QSAR model obtained using the LOO cross-validation method. Using both models, we predicted the activity of newly designed molecules, which showed pIC_{50} values ranging from 8.41 to 7.99 for the field-based QSAR model and from 8.32 to 8.01 for the atom-based QSAR model. Additionally molecular docking indicate that designed molecules exhibit interactions with crucial amino acids in the active site of β -secretase, reinforcing its

potential for further investigation as a β -secretase inhibitor. These findings lead us to the conclusion that both models are highly predictive and can be applied successfully in future studies.

Ethics

This was *in silico* study and did not directly involve with human participants or experimental animals. Therefore, the ethics approval was not required in this paper.

Acknowledgement

The authors would like to thank Dr N. D. Jivani, President, Dr Dinesh L. Sutaria, Secretary, Shree Dhanvantary Pharmacy College for providing necessary facilities.

Conflicts of interest

The authors declare that there is no conflict of interest.

Funding

This study was financially supported by DST-FIST, FIST PG College Level A - Project, New Delhi, India, Sanction Letter No SR/FST/College-/2022/1269 TPN 83823.

Data access

The data that support the findings of this study are available from the corresponding author upon reasonable individual request.

Author ORCID numbers

Uttam A More (UAM): 0000-0003-0436-8630
 Maitri Patel (MP): 0009-0003-9430-9331
 Krishna Patel (KP): 0009-0001-4883-3576
 Harsiddhi Patel (HP): 0009-0006-9559-1713
 Kruti Y. Patel (KYP): 0009-0006-6792-8446
 Neha Jain (NJ): 0009-0001-0496-9674
 Shabeena Khan (SK): 0009-0001-7707-6260
 Kinjal Vasandiya (KV): 0009-0008-3482-3052
 Malleshappa N Noolvi (MNN): 0000-0003-0497-6601
 Mahesh B Palkar (MBP): 0000-0001-7486-5275

Author contributions

Conceptualisation: UAM, MNN
 Methodology: UAM, KV, NJ
 Software: UAM
 Validation: UAM
 Formal analysis: KV, SK
 Investigation: KV, UAM
 Resources: MNN, SK, UAM,
 Data curation: MP, KP, HP, KYP
 Writing - original draft: MP, KP, HP, KYP
 Writing - review and editing: SK, NJ, KV, MBP
 Visualisation: UAM, MBP
 Supervision: UAM, MNN, MBP
 Project administration: UAM, MNN
 Funding acquisition: UAM, MNN

References

1. Blennow K, de Leon MJ, Zetterberg H. Alzheimer's disease. Lancet. 2006;368(9533):387-403. doi: 10.1016/S0140-6736(06)69113-7.
2. 2023 Alzheimer's disease facts and figures. Alzheimer Dement. 2023;19(4):1598-695. doi: 10.1002/alz.13016.
3. Vassar RJ. EC-01-03: Bace1, The beta-secretase enzyme: a leading therapeutic target for Alzheimer's disease. Alzheimer Dement. 2016;12:P162-P62. doi: 10.1016/j.jalz.2016.06.289.

4. Hardy J, Selkoe DJ. The amyloid hypothesis of Alzheimer's disease: progress and problems on the road to therapeutics. *Science*. 2002;297(5580):353-6. doi: 10.1126/science.1072994.
5. Menting KW, Claassen JAHR. β -secretase inhibitor; a promising novel therapeutic drug in Alzheimer's disease. *Front Aging Neurosci*. 2014;6:165. doi: 10.3389/fnagi.2014.00165.
6. Dislich B, Lichtenthaler SF. The membrane-bound aspartyl protease BACE1: molecular and functional properties in Alzheimer's disease and beyond. *Front Physiol*. 2012;3:8. doi: 10.3389/fphys.2012.00008.
7. Vassar R, Kovacs DM, Yan R, Wong PC. The β -secretase enzyme BACE in health and Alzheimer's disease: regulation, cell biology, function, and therapeutic potential. *J Neurosci*. 2009;29(41):12787-94. doi: 10.1523/JNEUROSCI.3657-09.2009.
8. Steiner H, Winkler E, Haass C. Chemical cross-linking provides a model of the gamma-secretase complex subunit architecture and evidence for close proximity of the C-terminal fragment of presenilin with APH-1. *J Biol Chem*. 2008 Dec 12;283(50):34677-86. doi: 10.1074/jbc.M709067200.
9. Patel S, Vuillard L, Cleasby A, Murray CW, Yon J. Apo and inhibitor complex structures of BACE (β -secretase). *J Mol Biol*. 2004;343(2):407-16. doi: 10.1016/j.jmb.2004.08.018.
10. Hong L, Tang J. Flap position of free memapsin 2 (β -secretase), a model for flap opening in aspartic protease catalysis. *Biochem*. 2004;43(16):4689-95. doi: 10.1021/bi0498252.
11. Hong L, Turner RT, Koelsch G, Shin D, Ghosh AK, Tang J. Crystal structure of memapsin 2 (β -secretase) in complex with an inhibitor OM00-3. *Biochem*. 2002;41(36):10963-67. doi: 10.1021/bi026232n.
12. Hong L, Koelsch G, Lin X, Wu S, Terzyan S, Ghosh AK, et al. Structure of the protease domain of memapsin 2 (beta-secretase) complexed with inhibitor. *Science*. 2000 Oct 6;290(5489):150-3. doi: 10.1126/science.290.5489.150.
13. Kim KH. Comparative molecular field analysis (CoMFA). In: Dean PM, ed. *Molecular similarity in drug design*. Dordrecht: Springer Netherlands, 1995; pp. 291-331. doi: 10.1007/978-94-011-1350-2_12.
14. Klebe G. Comparative molecular similarity indices analysis: CoMSIA. *Persp Drug Discovery Design* 1998;12(0):87-104 doi: 10.1023/A:1017025803403.
15. Kalva S, Vinod D, Saleena LM. Field-and Gaussian-based 3D-QSAR studies on barbiturate analogs as MMP-9 inhibitors. *Med Chem Res*. 2013;22:5303-13. doi: 10.1007/s00044-013-0479-6..
16. Klebe G. Quantitative Structure-Activity Relationships. In: Klebe G, ed. *Drug design: methodology, concepts, and mode-of-action*. Berlin, Heidelberg: Springer Berlin Heidelberg, 2013; pp. 371-96. doi: 10.1007/978-3-642-17907-5_18.
17. Wesnak N, Bhat SS, Romero AH. Structural exploration of low-energy Lennard-Jones-Gauss clusters with a genetic algorithm. *Eur Physical J B*. 2023;96(11):154. doi: 10.1140/epjb/s10051-023-00611-1.
18. Kumar SPJ, Susmita C, Sripathy KV, Agarwal DK, Pal G, Singh AN, et al. Molecular characterization and genetic diversity studies of Indian soybean (*Glycine max* (L.) Merr.) cultivars using SSR markers. *Mol Biol Rep*. 2022 Mar;49(3):2129-40. doi: 10.1007/s11033-021-07030-4.
19. Schrödinger LLC. Schrödinger Release 2017-1: Maestro. New York: Schrödinger LLC 2017.
20. Varpe BD, Jadhav SB, Chatale BC, Mali AS, Jadhav SY, Kulkarni AA. 3D-QSAR and Pharmacophore modeling of 3, 5-disubstituted indole derivatives as Pim kinase inhibitors. *Struct Chem*. 2020;31:1675-90. doi: 10.1007/s11224-020-01503-1.
21. Kharb R, Sharma PC, Yar MS. Pharmacological significance of triazole scaffold. *J Enzyme Inhib Med Chem*. 2011 Feb;26(1):1-21. doi: 10.3109/14756360903524304.